





ARTICLE

Pre-assembled Ca^{2+} entry units and constitutively active Ca^{2+} entry in skeletal muscle of calsequestrin-1 knockout mice

Antonio Michelucci^{1,2} , Simona Boncompagni^{2,3} , Laura Pietrangelo^{2,3}, Takahiro Takano¹, Feliciano Protasi^{2,4*} , and Robert T. Dirksen^{1*} 

Store-operated Ca^{2+} entry (SOCE) is a ubiquitous Ca^{2+} influx mechanism triggered by depletion of Ca^{2+} stores from the endoplasmic/sarcoplasmic reticulum (ER/SR). We recently reported that acute exercise in WT mice drives the formation of Ca^{2+} entry units (CEUs), intracellular junctions that contain STIM1 and Orai1, the two key proteins mediating SOCE. The presence of CEUs correlates with increased constitutive- and store-operated Ca^{2+} entry, as well as sustained Ca^{2+} release and force generation during repetitive stimulation. Skeletal muscle from mice lacking calsequestrin-1 (CASQ1-null), the primary Ca^{2+} -binding protein in the lumen of SR terminal cisternae, exhibits significantly reduced total Ca^{2+} store content and marked SR Ca^{2+} depletion during high-frequency stimulation. Here, we report that CEUs are constitutively assembled in extensor digitorum longus (EDL) and flexor digitorum brevis (FDB) muscles of sedentary CASQ1-null mice. The higher density of CEUs in EDL ($39.6 \pm 2.1/100 \mu\text{m}^2$ versus $2.0 \pm 0.3/100 \mu\text{m}^2$) and FDB ($16.7 \pm 1.0/100 \mu\text{m}^2$ versus $2.7 \pm 0.5/100 \mu\text{m}^2$) muscles of CASQ1-null compared with WT mice correlated with enhanced constitutive- and store-operated Ca^{2+} entry and increased expression of STIM1, Orai1, and SERCA. The higher ability to recover Ca^{2+} ions via SOCE in CASQ1-null muscle served to promote enhanced maintenance of peak Ca^{2+} transient amplitude, increased dependence of luminal SR Ca^{2+} replenishment on BTP-2-sensitive SOCE, and increased maintenance of contractile force during repetitive, high-frequency stimulation. Together, these data suggest that muscles from CASQ1-null mice compensate for the lack of CASQ1 and reduction in total releasable SR Ca^{2+} content by assembling CEUs to promote constitutive and store-operated Ca^{2+} entry.

Introduction

Store-operated Ca^{2+} entry (SOCE) is a ubiquitous Ca^{2+} influx mechanism triggered by depletion of intracellular Ca^{2+} stores (ER and SR). The main players of SOCE are (1) stromal interaction molecule-1 (STIM1), which senses Ca^{2+} levels within the lumen of the ER/SR (Roos et al., 2005; Zhang et al., 2005; Liou et al., 2005) and (2) Orai1, the Ca^{2+} release-activated Ca^{2+} channel in the plasma membrane (Feske et al., 2006; Vig et al., 2006; Yeromin et al., 2006; Prakriya et al., 2006). In skeletal muscle, SOCE was first reported by Steinhardt and colleagues in myotubes (Hopf et al., 1996) and subsequently by Kurebayashi and Ogawa (2001) in adult muscle fibers. Following their identification as the key players of SOCE in nonmuscle cells, STIM1 and Orai1 were also shown to mediate SOCE in skeletal muscle (Stiber et al., 2008; Lyfenko and Dirksen, 2008; Dirksen 2009).

STIM1/Orai1-dependent SOCE is proposed to be important in muscle growth and development, as well as in limiting fatigue during sustained activity (Stiber et al., 2008; Li et al., 2012; Wei-Lapierre et al., 2013; Carrell et al., 2016; Sztretye et al., 2017; Michelucci et al., 2018), although others have argued against a role of SOCE activation during muscle fatigue (Cully and Launikonis, 2013).

We recently reported that acute exercise promotes the formation of intracellular junctions between stacks of SR membranes and extensions of transverse tubule (TT) that contain STIM1 and Orai1 proteins (Boncompagni et al., 2017, 2018). As the formation of these SR/TT junctions correlates with both increased STIM1/Orai1 colocalization (Boncompagni et al., 2017) and enhanced SOCE function (Michelucci et al., 2019), they were

¹Department of Pharmacology and Physiology, University of Rochester School of Medicine and Dentistry, Rochester, NY; ²Center for Advanced Studies and Technologies, University G. d'Annunzio of Chieti, Chieti, Italy; ³Department of Neuroscience, Imaging and Clinical Sciences, University G. d'Annunzio of Chieti, Chieti, Italy; ⁴Department of Medicine and Ageing Sciences, University G. d'Annunzio of Chieti, Chieti, Italy.

*F. Protasi and R.T. Dirksen contributed equally to this article; Correspondence to Robert T. Dirksen: Robert_Dirksen@URMC.Rochester.edu

This work is part of the special collection entitled "Electrical Signaling in the Heart and Nervous System: A Joint Meeting of the Society of General Physiologists and Latin American Society of Biophysicists."

© 2020 Michelucci et al. This article is distributed under the terms of an Attribution–Noncommercial–Share Alike–No Mirror Sites license for the first six months after the publication date (see <http://www.rupress.org/terms/>). After six months it is available under a Creative Commons License (Attribution–Noncommercial–Share Alike 4.0 International license, as described at <https://creativecommons.org/licenses/by-nc-sa/4.0/>).

referred to as Ca^{2+} entry units (CEUs). Hence, CEUs are structures that assemble during acute exercise, when TTs extend from the triad to make contact with remodeled stacks of SR cisternae within the I band. CEUs are also dynamic as they disassemble over a few hours of recovery as TTs retract from SR stacks (Michelucci et al., 2019). This remodeling of the TT impacts muscle fiber function: TT elongation promotes increased constitutive and store-dependent Orail-mediated Ca^{2+} influx that promotes maintenance of Ca^{2+} transient amplitude and contractile force production during repetitive high-frequency stimulation. Importantly, these functional adaptations to acute exercise require the presence of functional Orail channels, as exercise does not induce these effects in either muscle-specific Orail knockout (KO) or dominant-negative Orail mice (Michelucci et al., 2019).

Calsequestrin-1 (CASQ1) is an acidic, high-capacity Ca^{2+} -binding protein located in the lumen of the SR terminal cisternae of fast-twitch muscle fibers (Campbell et al., 1983; Yano and Zarain-Herzberg, 1994). The primary role of CASQ1 is to buffer Ca^{2+} ions in order to maintain free Ca^{2+} levels inside the SR at a concentration of $\sim 400\text{--}500\ \mu\text{M}$ (Canato et al., 2010; Sztretye et al., 2011a; Ziman et al., 2010), while also providing a large accessible pool of available Ca^{2+} near sites of Ca^{2+} release during excitation-contraction coupling. In addition to being important for SR Ca^{2+} binding/storage, CASQ1 also modulates the activity of the ryanodine receptor-1 (RyR1), which functions as the main SR Ca^{2+} release channel in skeletal muscle during excitation-contraction coupling (Beard et al., 2002; Sztretye et al., 2011b). Ablation of CASQ1 results in structural remodeling of the triad and impaired intracellular Ca^{2+} handling (Paolini et al., 2007; Canato et al., 2010). Muscle fibers from CASQ1 KO (CASQ1-null) mice exhibit severely reduced releasable SR Ca^{2+} store content and enhanced susceptibility to rapid and deep SR Ca^{2+} depletion during sustained, high-frequency stimulation (Paolini et al., 2007; Canato et al., 2010; Sztretye et al., 2011b). CASQ1-deficiency also leads to an increased susceptibility of mice to hyperthermic crises during exposure to halogenated anesthetics, heat, and exercise (Dainese et al., 2009; Protasi et al., 2009; Michelucci et al., 2015, 2017; Guarnier et al., 2018) and mitochondrial alterations that progress to more severe structural damage with age (Paolini et al., 2015).

Recent evidence suggests that CASQ1 modulates SOCE (Shin et al., 2003; Zhao et al., 2010; Wang et al., 2015; Barone et al., 2017). Interestingly, in addition to a remodeling of the triad, muscle fibers from CASQ1-null mice exhibit stacks of SR membranes within the I-band region of the sarcomere that are remarkably similar to CEUs reported in muscle of WT mice following acute exercise (Boncompagni et al., 2012, 2017, 2018; Michelucci et al., 2019). Here we analyzed extensor digitorum longus (EDL) and flexor digitorum brevis (FDB) muscles from sedentary WT and CASQ1-null mice using a combination of ultrastructural (EM), biochemical (Western blot), and functional (Mn^{2+} quench of fura-2 fluorescence, intracellular Ca^{2+} measurements, ex vivo muscle contractility) approaches. These results suggest that skeletal muscle in sedentary CASQ1-null mice compensates for the loss of CASQ1 by increasing utilization of the external Ca^{2+} pool via preassembly of SR-TT junctions

within the I band (e.g., CEUs) that enhance both constitutive and store-dependent Ca^{2+} entry.

Materials and methods

Animals

4–6-mo-old male WT and CASQ1-null mice on congenic C57bl/6 background were housed in micro-isolator cages at 20°C in a 12-h light/dark cycle and provided free access to standard chow and water. All animal studies were designed to minimize animal suffering and were approved by the Italian Ministry of Health (313/2019-PR) and the University Committee on Animal Resources at the University of Rochester (UCAR2006-114E). Mice were sacrificed by exposure to CO_2 followed by cervical dislocation before dissection and removal of EDL and FDB muscles. For ex vivo contractility measurements, mice were first deeply anesthetized by intraperitoneal injection of $100\ \text{mg}\cdot\text{kg}^{-1}$ ketamine, $10\ \text{mg}\cdot\text{kg}^{-1}$ xylazine, and $3\ \text{mg}\cdot\text{kg}^{-1}$ acepromazine (Wei-Lapierre et al., 2013) before removal of EDL muscles and then sacrificed by cervical dislocation.

EM

Intact EDL and FDB muscles were fixed at room temperature with 3.5% or 6% glutaraldehyde in 0.1 M NaCaCo ($\text{C}_2\text{H}_6\text{AsNaO}_2$) buffer (pH 7.2) and processed for standard EM acquisition. For TT staining, muscle samples were post-fixed in a mixture of 2% OsO_4 and 0.8% potassium ferrocyanide ($\text{K}_3\text{Fe}(\text{CN})_6$) for 1–2 h followed by rinse with 0.1 M NaCaCo buffer with 75 mM CaCl_2 . Potassium ferrocyanide precipitate within the TT network is visualized as an electron-dense dark precipitate in EM images (Boncompagni et al., 2017). Ultrathin sections ($\sim 50\ \text{nm}$) were cut using a Leica Ultracut R microtome (Leica Microsystem) with a Diatome diamond knife (Diatome Ltd.) and double-stained with uranyl acetate and lead citrate. Sections were viewed in a FP 505 Morgagni Series 268D electron microscope (FEI Company) equipped with Megaview III digital camera and Soft Imaging Systemat 60 kV.

Quantitative analyses of EM images

The percentage of fibers exhibiting SR stacks and the number of SR stacks per $100\ \mu\text{m}^2$ were determined from electron micrographs of nonoverlapping regions randomly collected from transversal EM sections as described previously (Boncompagni et al., 2017; Michelucci et al., 2019). For each specimen, 10–15 representative fibers were analyzed, and five micrographs at $28,000\times$ magnification were taken for each fiber. The average length of SR stacks was measured in micrographs taken at $44,000\times$ magnification, while the number of membrane elements contained in each stack was obtained in micrographs taken at either $28,000\times$ or $44,000\times$ magnification. Extensions of the TT network within the I band of the sarcomere (total TT length), and TT/SR contact length (e.g., length of TT adjacent to SR stacks) were measured in electron micrographs of nonoverlapping regions randomly collected from transversal EM sections. For each specimen, 10–15 representative fibers were analyzed, and five micrographs at $28,000\times$ magnification were taken for each fiber. Quantitative analyses of SR stacks and TT

network extension were obtained using Analy-SIS software (Olympus Soft Imaging Solutions).

Isolation of single FDB muscle fibers

FDB muscles were dissected from hind paws and placed in a dish containing Ringer's solution consisting of 145 mM NaCl, 5 mM KCl, 2 mM CaCl_2 , 1 mM MgCl_2 , and 10 mM HEPES, pH 7.4. Muscles were then incubated in Ringer's solution supplemented with 1 mg/ml collagenase A (Roche) for 60 min while being rocked gently at 37°C to allow for enzymatic dissociation. Single FDB fibers obtained by mechanical dissociation/trituration were plated on glass-bottom dishes and allowed to settle for at least 20 min before single fiber experiments (detailed below). Only fibers with a clean morphology, clear striations, and no signs of swelling or damage were used.

Mn²⁺ quench measurements

For Mn²⁺ quench studies, acutely dissociated FDB fibers were loaded with 5 μM fura-2 AM (acetoxymethyl) ester for 1 h at 37°C in a Ca²⁺-free Ringer's solution containing 145 mM NaCl, 5 mM KCl, 3 mM MgCl_2 , and 0.2 mM EGTA, pH 7.4. To fully deplete SR Ca²⁺ stores (+depletion) before measurements of maximal rate of Mn²⁺ quench, fibers were incubated during fura-2 loading with two SERCA pump inhibitors (1 μM thapsigargin [TG]; 15 μM cyclopiazonic acid [CPA]) and a skeletal muscle myosin inhibitor (30 μM *N*-benzyl-*p*-toluene sulfonamide [BTS]) to prevent movement artifacts (Wei-Lapierre et al., 2013; Michelucci et al., 2019). In a second set of experiments, FDB fibers were loaded with fura-2 AM and BTS in the absence of SERCA pump inhibitors (−depletion). Both store-depleted and nondepleted fibers were then bathed in Ca²⁺-free Ringer's solution and excited at 362 nm (isobestic point of fura-2), while emission was detected at 510 nm using a DeltaRam illumination system (Photon Technologies Inc.). After obtaining an initial baseline rate of fura-2 decay (R_{baseline}), fibers were exposed to Ca²⁺-free Ringer's supplemented with 0.5 mM MnCl_2 . The maximum rate of change in fura-2 fluorescence in the presence of Mn²⁺ (R_{max}) was obtained from the peak time derivative of the fura-2 emission trace during Mn²⁺ application. The maximum rate of SOCE (R_{SOCE}) was calculated as $R_{\text{SOCE}} = R_{\text{max}} - R_{\text{baseline}}$ and expressed as change in fluorescence level with change (increase) in temperature (dF/dt) in counts per second, as described previously (Wei-Lapierre et al., 2013; Michelucci et al., 2019).

Ca²⁺ transient measurements

Myoplasmic Ca²⁺ transients were monitored in acutely isolated FDB fibers as previously described (Wei-Lapierre et al., 2013; Michelucci et al., 2019). Briefly, FDB fibers were loaded with 4 μM mag-fluo-4-AM, a rapid, low-affinity Ca²⁺ dye that maximizes resolution of Ca²⁺ transient magnitude and kinetics (Capote et al., 2005), for 30 min at room temperature followed by washout in dye-free solution supplemented with 25 μM BTS for 20 min. While continuously perfused with control Ringer's supplemented with 25 μM BTS, fibers were electrically stimulated with a repetitive stimulation protocol (40 consecutive, 500-ms duration, 50-Hz stimulus trains delivered every 2.5 s)

using an extracellular electrode placed adjacent to the fiber. Mag-fluo-4 was excited at 480 ± 15 nm using an Excite epifluorescence illumination system (Nikon Instruments), and fluorescence emission at 535 ± 30 nm was monitored using a 40× oil objective and photomultiplier detection system (Photon Technologies Inc.). Relative changes in mag-fluo-4 fluorescence from baseline (F/F_0) were recorded at 10 kHz and analyzed using Clampfit 10.0 (Molecular Devices).

SR free Ca²⁺ measurements

The free Ca²⁺ concentration in the SR lumen was assessed in single FDB fibers expressing the ER-targeted (DIER) cameleon Ca²⁺ sensor as described previously (Michelucci et al., 2019). DIER was expressed in FDB fibers by electroporation as previously described (Canato et al., 2010; Michelucci et al., 2019). Briefly, hind limb footpads of anesthetized mice were first injected with bovine hyaluronidase (6 μl , 0.4 U/ μl) and then 1 h later with DIER cDNA (20 μg in 71 mM NaCl) using 30-gauge needles. The footpad was then electroporated with 20 stimulations of 100 V/cm, 20-ms duration delivered at 1 Hz using subcutaneous electrodes placed perpendicularly to the long axis of the muscle, close to the proximal and distal tendons. Fibers were isolated and used for experiments 7–14 d later. DIER-expressing fibers were bathed in control Ringer's solution supplemented with 25 μM BTS and placed on the stage of an inverted Nikon Eclipse TE-2000-U microscope (Nikon Instruments). A rectangular region of interest of the fiber was excited at 436 nm (10 nm bandwidth). Fluorescence emission within the region of interest was split with a 515-nm dichroic mirror and collected at 480 nm (30 nm bandwidth) and 535 nm (30 nm bandwidth) using a photomultiplier counting system (Photon Technologies Inc.). DIER emission was continuously monitored before, during, and after each stimulus of a repetitive stimulation protocol (40 consecutive, 500 ms duration, 50 Hz stimulus trains delivered every 2.5 s). To directly compare measurements across multiple fibers, all experiments used identical excitation and emission gains. Both 480-nm and 535-nm fluorescence signals were collected and digitized at 100 Hz. The ratio of the two emissions ($R = F_{535}/F_{480}$) was calculated using Clampex 10 (Molecular Devices). The change in ratio during each stimulation train was obtained by subtracting the average of 50 ms before the start of the stimulation from the average of 50 ms at the end of the stimulation using Clampfit 10 (Molecular Devices).

Total Ca²⁺ store content measurements

Total releasable Ca²⁺ store content was determined in FDB fibers loaded with 4 μM fura-FF AM, a low-affinity ratiometric Ca²⁺ dye, for 30 min at room temperature in control Ringer's solution followed by 30 min washout in dye-free Ringer's solution supplemented with 40 μM BTS as described previously (Loy et al., 2011; Michelucci et al., 2019). Fibers were then perfused in Ca²⁺-free Ringer's solution while alternately excited at 340 and 380 nm (510-nm emission) every 250 ms (30-ms exposure per wavelength and 2×2 binning) using a monochromator-based illumination system (TILL Photonics). Fura-FF emission at 535 ± 30 nm was captured using a high-speed, digital QE charge-coupled device camera (TILL Photonics). Total releasable Ca²⁺ store

content was assessed from the difference between baseline and peak fura-FF ratio ($\Delta\text{Ratio}_{340/380}$) upon application of a Ca^{2+} release cocktail containing 10 μM ionomycin, 30 μM CPA, and 100 μM EGTA in a Ca^{2+} -free Ringer's solution (ionomycin-CPA-EGTA; ICE) for a period of 60 s. The exposure to ICE releases Ca^{2+} from intracellular Ca^{2+} storage compartments, which is dominated in muscle by the SR. The decay of the signal after the peak reflects a combination of activation of Ca^{2+} efflux mechanisms (e.g., plasma membrane Ca^{2+} ATPase, Na/Ca exchange) and in some cases movement artifacts due to a slowly developing fiber hypercontracture. As a result, while the peak of the ICE response for a given condition is reproducible, the decay phase is complex and variable. To confirm that the peak of the fura-FF signal during ICE application was not saturated, maximal fura-FF responsiveness was assessed at the end of each experiment by subsequent application of Ca^{2+} -containing Ringer's solution. Analysis of the peak ICE-induced change in fura-FF ratio ($\Delta\text{Ratio}_{340/380}$) was calculated using Clampfit 10.0 (Molecular Devices).

Ex vivo fatigue assay

Ex vivo assessment of muscle force production was made in intact excised EDL muscles attached to a servo motor and force transducer 1200 A (Aurora Scientific) and electrically stimulated using two platinum electrodes in a chamber continuously perfused with oxygenated Ringer's solution at 30°C (Michelucci et al., 2019). Optimal stimulation and muscle length (L_0) were determined using a series of 1-Hz twitch stimuli while stretching the muscle to a length that generated maximal force (F_0). After establishing L_0 , muscles were equilibrated using three tetani (500 ms, 150 Hz) given at 1-min intervals and then subjected to a standard force frequency protocol (from 1 to 250 Hz). After an additional 5 min of rest, muscles were then subjected to a repetitive stimulation protocol (40 consecutive, 500-ms duration, 50-Hz stimulus trains delivered every 2.5 s). Muscle force was recorded using Dynamic Muscle Control software and analyzed using a combination of Dynamic Muscle Analysis (Aurora Scientific) and Clampfit 10.0 (Molecular Devices) software. Specific force was calculated by normalizing the absolute force to the physiological cross-sectional area as previously described (Boncompagni et al., 2017; Michelucci et al., 2019).

Western blot

EDL muscles were excised, snap-frozen in liquid nitrogen, and homogenized in radioimmunoprecipitation assay lysis buffer (20 mM Tris-HCl, 150 mM NaCl, 1 mM Na_2EDTA , 1 mM EGTA, 1% nonyl phenoxypolyethoxyethanol-40, 1% Na-deoxycholate, 2.5 mM Na-pyrophosphate, 1 mM b-glycerophosphate, 1 mM Na_2VO_4 , and 1 $\mu\text{g}/\text{ml}$ leupeptin, pH 7.5) supplemented with a cocktail of protease inhibitors. Protein concentration was determined spectrophotometrically using the Lowry method. Briefly, 10 μg of total protein was loaded in each lane of 10% polyacrylamide electrophoresis gels, transferred to nitrocellulose membrane, and blocked with 5% nonfat dry milk (BioRad) in Tris-buffered saline 0.1% and Tween 20 (TBS-T) for 1–1.5 h. Membranes were probed with one of the following primary antibodies diluted in 5% nonfat dry milk in TBS-T overnight at

4°C: STIM1 antibody (rabbit polyclonal 1:5,000; Sigma-Aldrich); SERCA1/2/3 (rabbit polyclonal 1:10,000; Santa Cruz Biotechnology); Orail (mouse monoclonal 1:1,000; Santa Cruz Biotechnology); glyceraldehyde-3-phosphate dehydrogenase antibody (mouse monoclonal 1:50,000; Invitrogen). Membranes were washed three times in TBS-T and incubated with secondary antibodies (goat anti-mouse IgG-800 and goat anti-rabbit IgG-800 1:10,000; Invitrogen) diluted in 5% nonfat dry milk in TBS-T for 1 h at room temperature. Proteins were visualized using an Odyssey Infra-red Imager (Li-Cor Biosciences). Quantitative analyses were performed on exported TIFF images using Image J software (National Institutes of Health).

Statistical analyses

Statistical significance was determined using either unpaired two-tailed Student's *t* test when comparing means between two groups or ANOVA followed by the post hoc Tukey test for repeated measures (e.g., time-course analysis of Ca^{2+} transient amplitudes during repetitive, high-frequency stimulation). Unpaired two-tailed Student's *t* test and ANOVA followed by post hoc Tukey test for repeated measures were performed using OriginLab software (OriginLab Corp). In all cases, differences were considered as statistically significant at *, $P < 0.05$. All data were presented as mean \pm SEM.

Online supplemental material

Fig. S1 summarizes SR-stack incidence, number/area, and TT extension in FDB muscle fibers. Fig. S2 shows *N*-[4-[3,5-bis(trifluoromethyl)pyrazol-1-yl]phenyl]-4-methylthiadiazole-5-carboxamide (BTP-2) sensitivity of store-operated and constitutive Mn^{2+} quench in FDB fibers. Fig. S3 depicts mag-fluo-4 fluorescence tail integrals and end/peak ratios during repetitive stimulation. Fig. S4 presents contractile specific force and decay during repetitive stimulation of EDL muscles from CASQ1-null mice in the presence or absence of extracellular Ca^{2+} influx. Fig. S5 shows double immunostaining for RyR1 and Orail in EDL fibers.

Results

Muscle fibers from CASQ1-null mice contain preassembled SR-TT junctions within the I band of the sarcomere

Acute exercise induces a remodeling of the SR in skeletal muscle into flat stacks of cisternae and extension of TTs to form new junctions within the I band (Boncompagni et al., 2017, 2018; Michelucci et al., 2018, 2019). Here, we quantified the incidence and size of stacks of SR membranes in EM images of cross and longitudinal sections in EDL muscle fibers from sedentary WT and CASQ1-null mice (Fig. 1). While SR stacks were rarely observed in muscle from WT mice (Fig. 1, A and C), they were relatively abundant in muscle from CASQ1-null mice (Fig. 1, B and D), with a significantly higher percentage of fibers exhibiting SR stacks (Fig. 1 E) and stacks per unit area (100 μm^2 ; Fig. 1 F). We also evaluated the size of SR stacks by measuring their length and the number of elements in each stack (indicated respectively with blue dots and numbers in Fig. 1, C and D). SR stacks were significantly longer (Fig. 1 G) and contained a higher number of elements (Fig. 1 H) in muscle from CASQ1-null mice

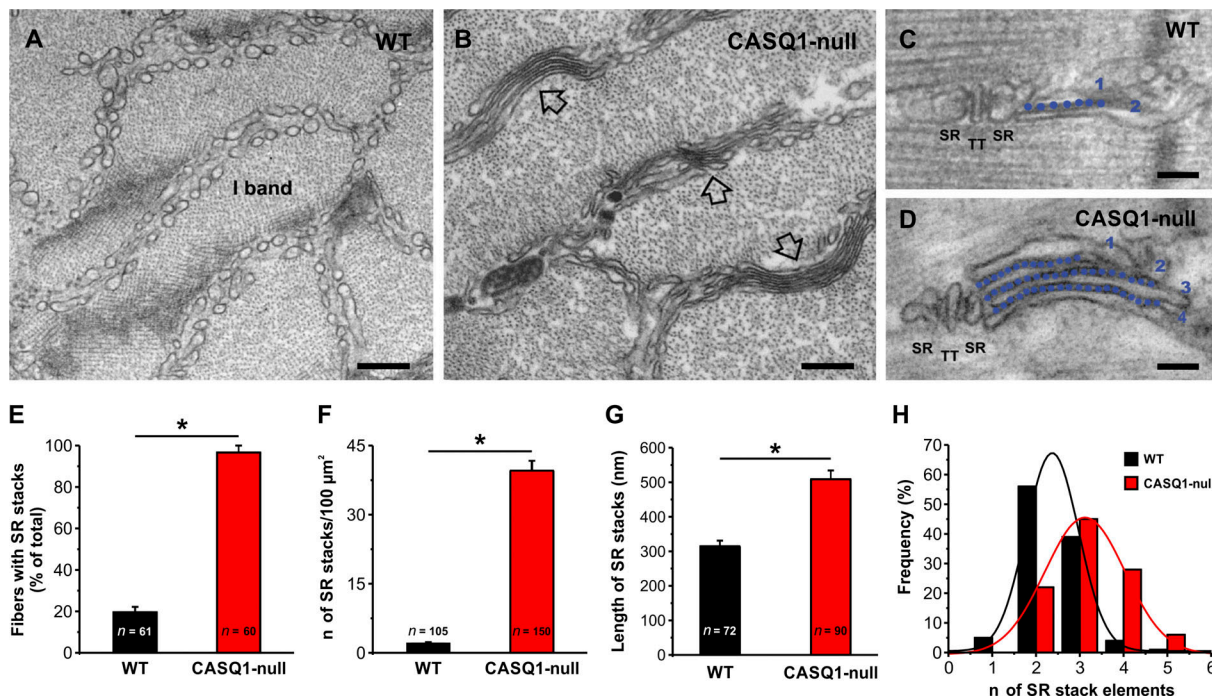


Figure 1. Incidence and size of SR stacks. (A and B) Representative EM images of cross sections of EDL muscle fibers from WT (A) and CASQ1-null (B) mice (empty arrows point to stacks of SR membranes). (C and D) Representative EM images of longitudinal sections of EDL muscle fibers showing stacks of SR membranes in proximity to triads (SR-TT-SR). (E–H) Quantitative analyses of the percentage of muscle fibers exhibiting SR stacks (E), the number of SR stacks per 100 μm² of cross-sectional area (F), the average SR stack length (G; labeled by dots in C and D), and the frequency of the number of SR stack elements (H; numbered in C and D) in EDL muscles WT and CASQ1-null mice. Data are shown as mean ± SEM; *, $P < 0.05$. Numbers in bars (n) indicate the number of fibers analyzed. Number of mice: $n = 4$ WT; $n = 4$ CASQ1-null. Data for EDL muscles from WT mice shown in E–G are the same as those reported in Boncompagni et al. (2017) and Michelucci et al. (2019). Scale bars: 0.2 μm, A and B; 0.1 μm, C and D.

compared with that observed for WT mice. A similar increase in both the percentage of fibers with SR stacks and the number of SR stacks per unit area was also observed in FDB muscle fibers (Fig. S1, A and B).

Since acute exercise induces elongation of TTs into SR stacks in the I band (Boncompagni et al., 2017; Michelucci et al., 2019), we also quantified the total TT length and extent of contact with flat-parallel stacks of SR within the I band in EDL muscles post-fixed in the presence of ferrocyanide. Ferrocyanide forms a dark precipitate that enables direct visualization of TTs as dark structures in EM sections (see Materials and methods for further details). Representative EM images revealed that while TT extensions into the I band were rare in muscle fibers from WT mice (Fig. 2, A and B), they were more frequent and branched in muscle from CASQ1-null mice (Fig. 2, C and D). Quantitative analyses confirmed that TT length/100 μm² was approximately five times greater (Fig. 2 E) and TT/SR-stack contact length (Fig. 2 F) was increased ~10 times in muscle fibers from CASQ1-null mice compared with that of WT mice. Similar results were observed in FDB muscle fibers (Fig. S1 C).

Constitutive and store-operated Ca^{2+} entry is increased in FDB fibers from CASQ1-null mice

Acute exercise induces assembly of CEUs that correlates with: (1) increased colocalization of STIM-Orai1 at the I band (Boncompagni et al., 2017); (2) enhanced constitutive and store-

operated Ca^{2+} entry (Michelucci et al., 2019); and (3) increased ability to maintain peak Ca^{2+} transient amplitude and contractile force during repetitive stimulation (Boncompagni et al., 2017; Michelucci et al., 2019). Since preassembled SR-TT junctions at the I band in CASQ1-null mice resemble CEUs assembled in WT mice following acute exercise, we measured the maximum rate of Mn^{2+} quench of fura-2 fluorescence in FDB fibers from CASQ1-null mice as an index of Ca^{2+} entry (Wei-Lapierre et al., 2013; Michelucci et al., 2019). Mn^{2+} quench experiments were performed both following SR Ca^{2+} store depletion (+depletion) to maximally activate SOCE (Fig. 3, A, C, and E) and in the absence of store depletion (–depletion) to assess constitutive Ca^{2+} entry (Fig. 3, B, D, and F). Following TG/CPA-induced SR depletion, FDB fibers from both WT and CASQ1-null mice exhibited significant Mn^{2+} quench upon application of 0.5 mM extracellular Mn^{2+} (Fig. 3 A). However, the maximum rate of Mn^{2+} quench following store depletion (SOCE) was approximately two times larger in fibers from CASQ1-null mice (Fig. 3, C and E). In the absence of prior TG/CPA-induced Ca^{2+} store depletion, the fura-2 fluorescence emission was unaltered upon addition of Mn^{2+} in FDB fibers from WT mice, whereas a significant quench was observed in FDB fibers from CASQ1-null mice (Fig. 3 B), consistent with the presence of a constitutive Ca^{2+} entry mechanism in these fibers (Fig. 3, D and F). Interestingly, the magnitude of constitutive Mn^{2+} quench in FDB fibers from sedentary CASQ1-null mice ($2.0 \pm 0.3 \times 10^3$ counts/s; Fig. 3 D) was even larger than that reported previously in FDB fibers from WT mice after acute

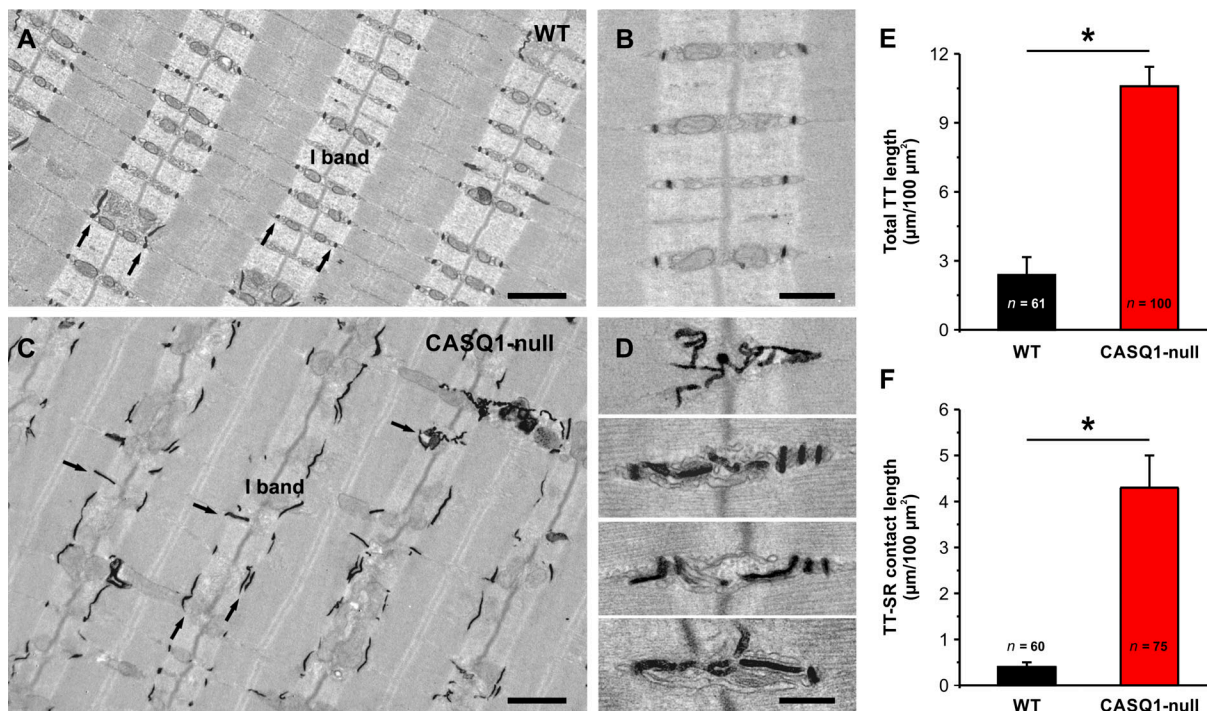


Figure 2. TT extension and TT/SR stack contact lengths. (A–D) Representative EM images of longitudinal sections of EDL muscle fibers from WT (A and B) and CASQ1-null (C and D) mice showing TTs stained in black with ferrocyanide precipitate. (E and F) Quantitative analyses of total TT length (E) and TT-SR contact length (F) per 100 μm^2 of cross-sectional area in EDL muscle from WT and CASQ1-null mice. Data are shown as mean \pm SEM; *, $P < 0.05$. Numbers in bars (n) indicate the number of EDL fibers analyzed. Number of mice: $n = 4$ WT; $n = 4$ CASQ1-null. Data for EDL muscles from WT mice shown in E and F are the same as those reported by Boncompagni et al. (2017) and Michelucci et al. (2019). Scale bars: 1 μm , A and C; 0.5 μm , B and D.

exercise ($1.2 \pm 0.2 \times 10^3$ counts/s; Michelucci et al., 2019). Similar to what was reported for FDB fibers from acutely exercised WT mice, the enhanced store-operated and constitutive Ca^{2+} entry observed in FDB fibers from CASQ1-null mice were rapidly inhibited by acute application of 10 μM BTP-2 (Fig. S2), a SOCE channel inhibitor (Zitt et al., 2004).

STIM1, Orai1, and SERCA expression are increased in muscle of CASQ1-null mice

Given the increase in constitutive and store-operated Ca^{2+} entry in muscle fibers from CASQ1-null mice, we compared STIM1, Orai1, and SERCA protein levels in EDL muscle homogenates from WT and CASQ1-null mice (Fig. 4). These analyses revealed that relative expression of both STIM1S and STIM1L (the short and long splice variants of STIM1, respectively) were significantly increased (60–70%) in CASQ1-null mice (Fig. 4, A, D, and E). An ~ 2.5 -fold increase in Orai1 was also observed (Fig. 4, B and F), with the specificity of the Orai1 antibody validated by the lack of reactivity in EDL samples from constitutive, muscle-specific Orai1 KO mice (cOrai1 KO). We also evaluated relative expression of SERCA, the Ca^{2+} ATP-ase pump responsible for Ca^{2+} reuptake from the myoplasm back into the SR lumen during relaxation. Similar to STIM1 and Orai1, quantitative analyses revealed a modest ($\sim 25\%$) but statistically significant increase of SERCA expression in EDL muscle from CASQ1-null mice (Fig. 4, C and G), consistent with prior reports of increased SERCA activity in muscle from these mice (Guarnier et al., 2018).

Peak Ca^{2+} transient amplitude during repetitive stimulation is enhanced in FDB fibers from CASQ1-null mice

To determine the impact of increased constitutive and store-operated Ca^{2+} entry on the ability of muscle fibers to sustain Ca^{2+} release during repetitive stimulation, myoplasmic Ca^{2+} transients elicited during 40 consecutive high-frequency stimulus trains (50 Hz, 500 ms, every 2.5 s) were recorded in FDB fibers isolated from WT and CASQ1-null mice. While peak Ca^{2+} transient amplitude during the first stimulus train was not different between fibers from WT and CASQ1-null mice, a marked decay in Ca^{2+} transient amplitude occurred in fibers from CASQ1-null mice (Fig. 5 A, left). During subsequent stimulus trains, the temporal evolution of peak Ca^{2+} transient amplitudes was markedly different between fibers from WT and CASQ1-null mice (Fig. 5, A and B). In particular, fibers from WT mice exhibited a relatively modest increase in peak Ca^{2+} transient amplitude (or bump phase) for a few stimuli after the first stimulus train followed by a steady reduction after the fourth stimulus train. Conversely, fibers from CASQ1-null mice exhibited a marked reduction in Ca^{2+} transient amplitude during the second stimulus train followed by a more pronounced and sustained bump phase (Fig. 5 B). Quantitative analyses revealed that both the decrement in Ca^{2+} transient amplitude during the second stimulus train and the magnitude of the bump phase were significantly greater in FDB fibers from CASQ1-null mice (Fig. 5 C). We also quantified the decay phase of the Ca^{2+} transient following termination of each stimulus train by integrating the area under the curve of the fluorescence trace (“tail integral,” hatched area shown in light gray in

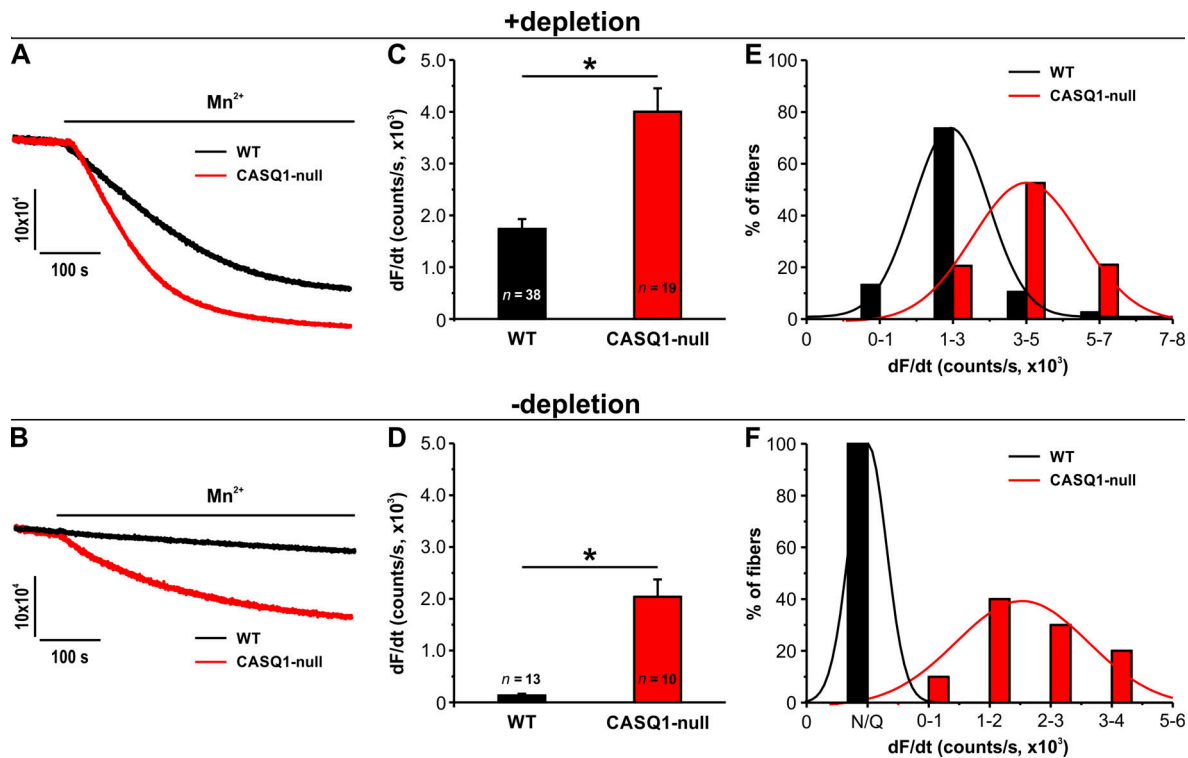


Figure 3. Maximum rate of Mn^{2+} quench in the presence or absence of store depletion. (A and B) Representative traces of fura-2 fluorescence during application of 0.5 mM Mn^{2+} in FDB fibers isolated from WT and CASQ1-null mice following prior store depletion induced with 1 μM TG + 15 μM CPA (A; +depletion) and in the absence of store depletion (B; -depletion). (C and D) Quantitative analyses of the maximum rate of Mn^{2+} quench in the presence (C) and absence (D) of prior store depletion. (E and F) Frequency histograms of the percentage of FDB fibers exhibiting different levels of maximum rate of Mn^{2+} quench in the presence (E) and absence (F) of prior store depletion. Histogram data were fit with a single Gaussian distribution. Data are shown as mean \pm SEM; * $P < 0.05$. Numbers in bars (n) indicate the number of FDB fibers analyzed. Number of mice: $n = 6$ WT; $n = 5$ CASQ1-null.

Fig. S3 A). Assuming Ca^{2+} release ends upon termination of the stimulation, the tail integral reflects the balance of Ca^{2+} influx (e.g., SOCE) and removal (e.g., SERCA, plasma membrane Ca^{2+} ATPase), as reported previously (Wei-Lapierre et al., 2013). While the tail integral decreased steadily during repetitive stimulation in fibers from WT mice, it increased in fibers from CASQ1-null mice (Fig. S3, B and D). The end/peak ratio of the Ca^{2+} transient during the stimulus train (peak Ca^{2+} transient at the end or Peak_{end}) divided by the peak value at the beginning (Peak_{initial}; Fig. S3 A, right) provides information regarding the kinetics of Ca^{2+} transient decline (e.g., end/peak ratio of 1.0 represents no decay). This analysis revealed a steady increase in end/peak ratio (or reduction in Ca^{2+} transient decay with each stimulus train) only in fibers from CASQ1-null mice (Fig. S3, B and D).

Total Ca^{2+} store content is reduced while BTP-2-sensitive store refilling during repetitive stimulation is increased in FDB fibers from CASQ1-null mice

As SOCE is a mechanism activated by the depletion of intracellular Ca^{2+} stores, we measured total Ca^{2+} store content under resting conditions (e.g., without electrical stimulation) and dynamic changes in free luminal SR Ca^{2+} concentration during repetitive stimulation (Fig. 6). Total Ca^{2+} store content was assessed in FDB fibers loaded with fura-FF during application of a Ca^{2+} store release cocktail (ICE; Fig. 6 A). Assessed in this way, total Ca^{2+} store content in FDB fibers from CASQ1-null mice was

<10% of that observed in FDB fibers from WT mice (Fig. 6 B). We also compared SR free Ca^{2+} concentration in FDB fibers expressing the DIER cameleon luminal SR Ca^{2+} sensor (Michelucci et al., 2019). Confocal microscopy of immunofluorescence staining revealed that the majority of the DIER signal was localized to the terminal cisternae of the SR (at the triad junction), on either side of the Z-line (immunostained for α -actinin in red; Fig. 6 C). Spatially averaged measurements of DIER emission (Fig. 6 D) indicated that terminal SR luminal Ca^{2+} levels were modestly elevated in fibers from CASQ1-null mice under resting conditions, a difference that was abolished by preincubation with 10 μM BTP-2 (Fig. 6 E). To assess luminal free Ca^{2+} dynamics during repetitive stimulation, we measured changes in DIER_{535/480} emission ratio during repetitive stimulation with the same protocol used in Fig. 5. Consistent with previous observations (Canato et al., 2010), electrical stimulation at 50 Hz promoted a marked reduction in luminal free Ca^{2+} levels in FDB fibers from CASQ1-null (but not WT) mice, as indicated by the deep reduction in DIER_{535/480} ratio at the end of the first stimulus train (Fig. 6 D). Importantly, while DIER_{535/480} ratio remained stable throughout repetitive stimulation of fibers from WT mice, a progressive rebound increase was observed in fibers from CASQ1-null mice (Fig. 6 F). This progressive increment in DIER_{535/480} ratio during repetitive stimulation paralleled the pronounced bump phase of the peak Ca^{2+} transient observed during repetitive stimulation and was significantly reduced by pretreatment with 10 μM BTP-2 (Fig. 6 F).

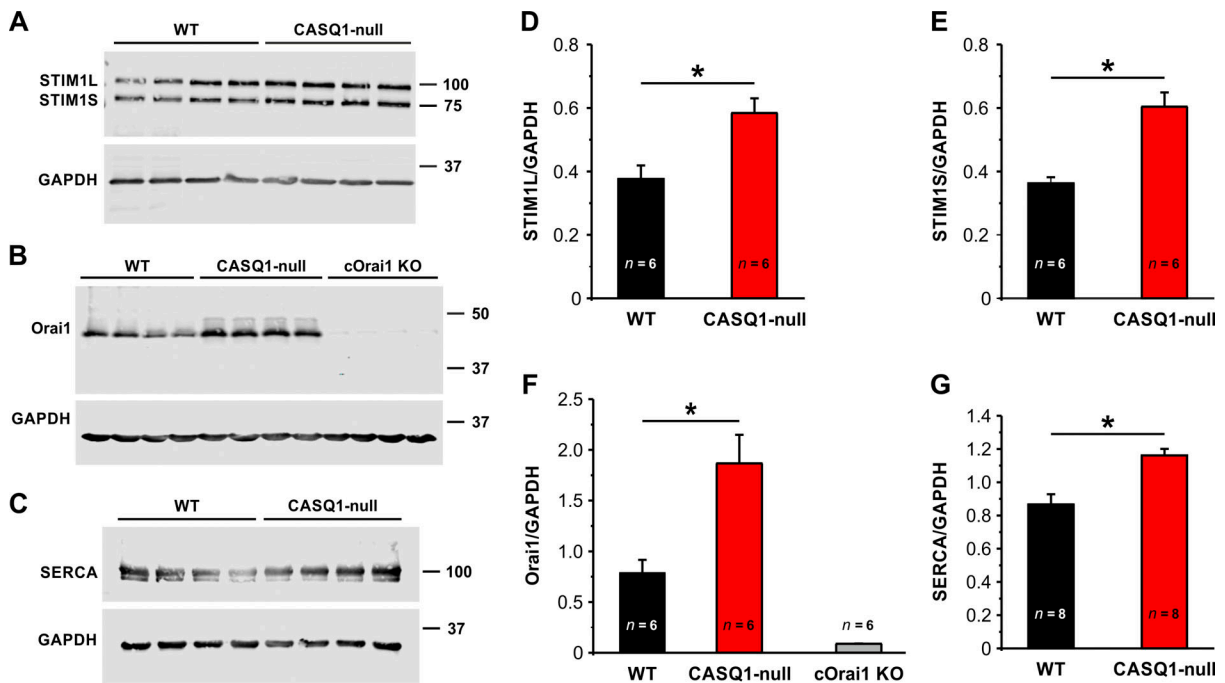


Figure 4. Western blot analyses of proteins that coordinate SOCE and SR Ca^{2+} uptake. (A–C) Representative immunoblots showing expression levels of the long (STIM1L) and short (STIM1S) STIM1 isoforms (A), Orai1 (B), and SERCA (C) in EDL muscle homogenates from WT and CASQ1-null mice. For Orai1 expression, EDL muscles from constitutive, muscle-specific Orai1 KO (cOrai1 KO) mice were used as a control for validation of the Orai1 antibody employed. **(D–G)** Relative band intensities (normalized to glyceraldehyde 3-phosphate dehydrogenase antibody [GAPDH]) for each of the proteins shown in A. Data are shown as mean \pm SEM; *, $P < 0.05$. Numbers in bars (n) indicate the number of mice analyzed.

Peak specific force during repetitive stimulation is enhanced and dependent on extracellular Ca^{2+} entry in EDL muscle from CASQ1-null mice

To determine if both the enhanced constitutive/store-operated Ca^{2+} entry and Ca^{2+} release during repetitive stimulation observed in muscle fibers from CASQ1-null mice correlated with

an increased ability to maintain contractile force, intact EDL muscles were subjected to the same repetitive stimulation protocol used for dissociated single FDB fibers in Fig. 5 and Fig. 6. Specific force was measured in standard Ringer's solution (containing 2.5 mM Ca^{2+}) and also under conditions designed to reduce Ca^{2+} entry (e.g., 0 Ca^{2+} and 10 μM BTP-2; Fig. 7). Similar

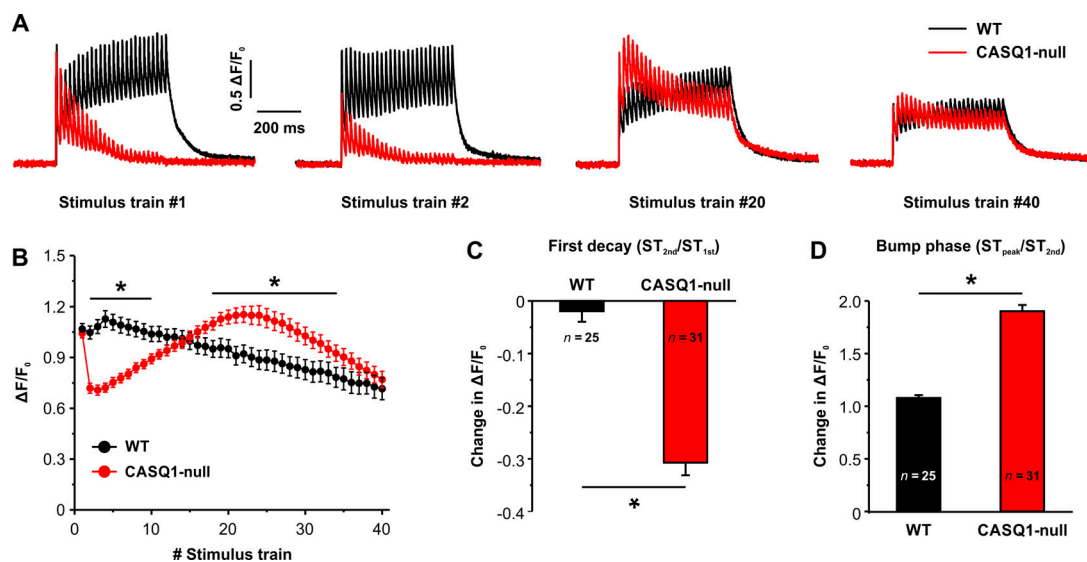


Figure 5. Ca^{2+} transients during repetitive stimulation. (A) Representative mag-fluo-4 ($\Delta F/F_0$) traces during the 1st, 2nd, 20th, and 40th stimulus trains in FDB fibers from WT and CASQ1-null mice. **(B)** Time course of relative change in peak mag-fluo-4 fluorescence during 40 consecutive stimulus trains. **(C and D)** Quantitative analyses of the relative decay during the second stimulus train (ST_{2nd}/ST_{1st} ; C) and the peak of the bump phase (ST_{peak}/ST_{2nd} ; D) from the data shown in B. Data are shown as mean \pm SEM; *, $P < 0.05$. Numbers in bars (n) indicate the number of FDB fibers analyzed. Number of mice: $n = 4$ WT; $n = 5$ CASQ1-null.

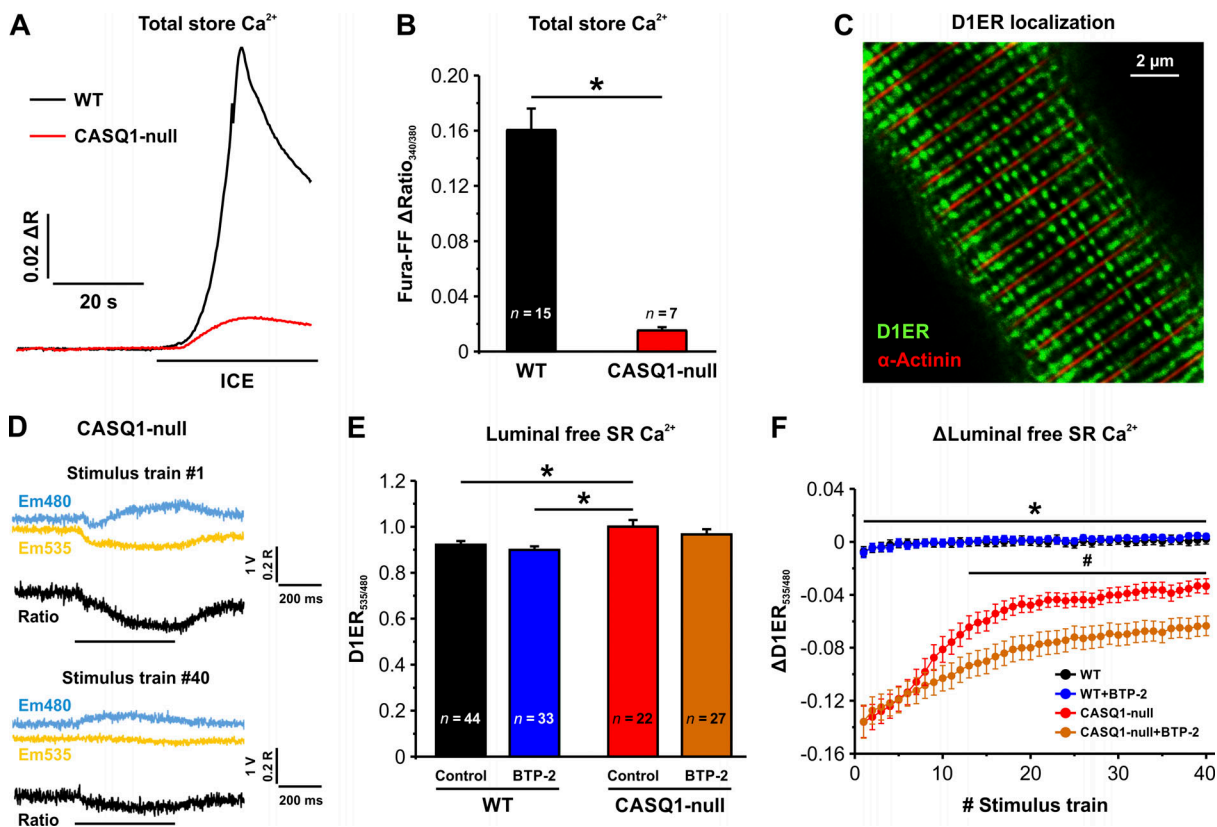


Figure 6. Measurements of total releasable Ca^{2+} store content and luminal free SR Ca^{2+} . (A and B) Representative superimposed fura-FF fluorescence traces (A) and quantitative analyses of total releasable Ca^{2+} store content (B) elicited during application of Ca^{2+} release cocktail (ICE). (C) Representative immunofluorescence confocal image for D1ER (green) and α -actinin (red) in an FDB fiber from a WT mouse. (D) Representative D1ER emission (Em₄₈₀ and Em₅₃₅) and D1ER_{535/480} ratio traces during the 1st (upper) and 40th (lower) stimulus train recorded from a representative FDB fiber of a CASQ1-null mouse. (E and F) Quantitative analyses of the average resting D1ER ratio (D1ER_{535/480}; E) and time course change of D1ER_{535/480} during 40 consecutive stimulus trains (F) in FDB fibers from WT and CASQ1-null mice in the presence or absence of 10 μM BTP-2. Data are shown as mean \pm SEM; *, $P < 0.05$, WT compared with both CASQ1-null and CASQ1-null + BTP-2. #, $P < 0.05$, CASQ1-null compared with CASQ1-null + BTP-2. Numbers in bars (n) indicate the number of FDB fibers analyzed. Number of mice: $n = 6$ WT; $n = 4$ WT + BTP-2; $n = 3$ CASQ1-null; $n = 3$ CASQ1-null + BTP-2.

to that observed for Ca^{2+} transients (Fig. 5), peak specific force in EDL muscles from WT and CASQ1-null mice was not different during the first stimulus train (Fig. 7 A), although a marked decay in force was observed during the 500-ms stimulus train (Fig. S4 A). In addition, EDL muscles from CASQ1-null mice exhibited a greater drop in specific force during the second stimulus train but a more pronounced rebound bump phase compared with muscles from WT mice (Fig. 7, A and D). The reduction in specific force during the second stimulus (ratio between specific force produced during the second and first stimuli or $\text{ST}_{2\text{nd}}/\text{ST}_{1\text{st}}$) and magnitude of the rebound bump phase (ratio between peak specific force produced during the peak and second stimuli or $\text{ST}_{\text{peak}}/\text{ST}_{2\text{nd}}$) were significantly larger in EDL muscles from CASQ1-null mice (Fig. 7, A and D). As a result of the more prominent and sustained bump phase, peak specific force was significantly greater in EDL muscles from CASQ1-null mice after the 20th stimulus train.

Parallel measurements were also performed under conditions designed to limit/block Ca^{2+} entry including (1) nominally Ca^{2+} -free Ringer's solution (equimolar replacement with Mg^{2+} ; Fig. 7, B and E); and (2) standard Ca^{2+} -containing Ringer's

solution supplemented with 10 μM BTP-2 (Fig. 7, C and F). Consistent with previous studies (Boncompagni et al., 2017), these interventions exhibited only modest, but statistically significant, effects on specific force production of EDL muscles from WT mice during repetitive stimulation (Fig. 7, B, C, E, and F). On the other hand, these interventions dramatically increased the reduction in specific force production observed during the second stimulus and essentially abolished the rebound bump phase during subsequent stimulations in CASQ1 null fibers (Fig. 7, B, C, E, and F; and Fig. S4, A and B). In addition, while the prominent contractile decline observed during each stimulus train in EDL muscles from CASQ1-null mice recorded in normal Ringer's solution (end/peak ratio) is progressively reduced during the rebound bump phase, this phenomenon was also markedly diminished by interventions that prevent Ca^{2+} entry (Fig. S4 C).

Discussion

Main findings

The total amount of releasable Ca^{2+} from intracellular stores is markedly reduced and the SR undergoes severe depletion when

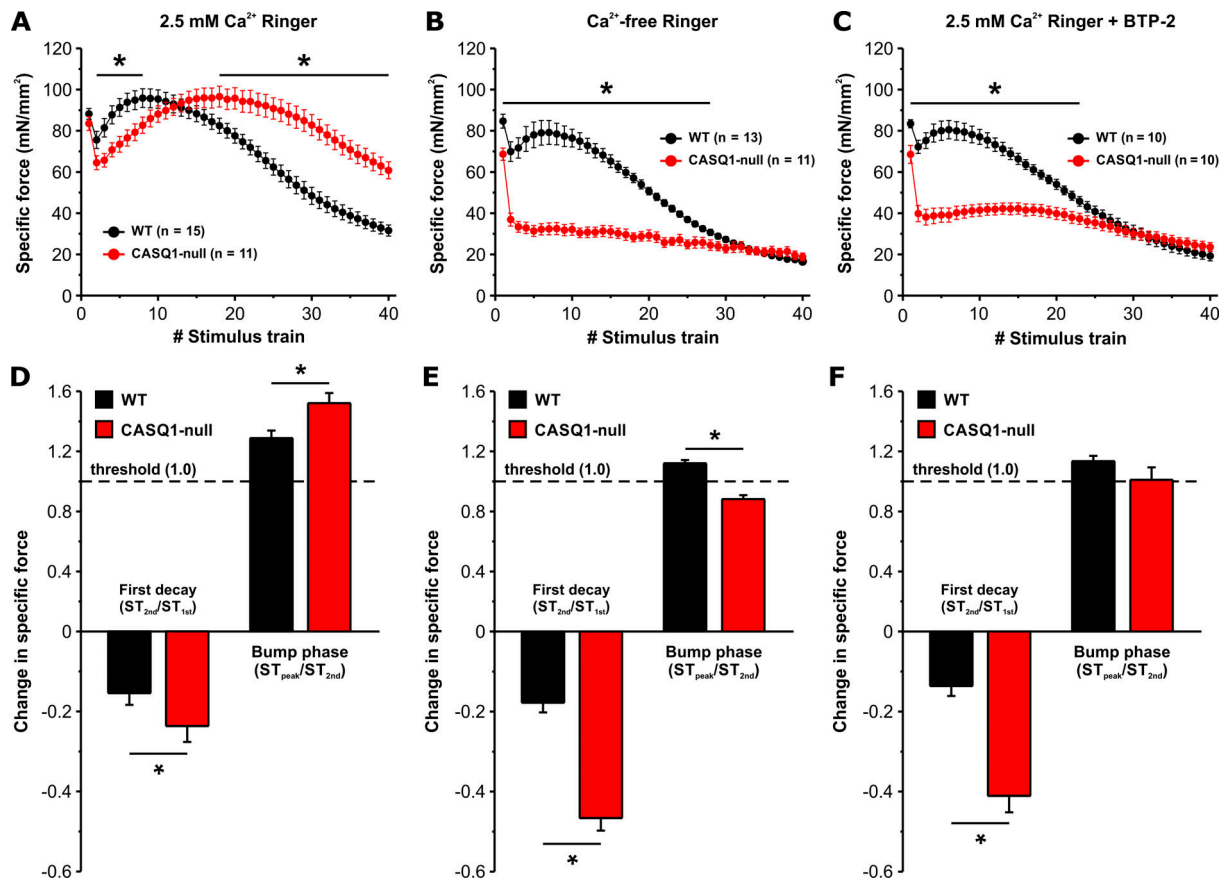


Figure 7. Contractile force during repetitive stimulation in the presence or absence of extracellular Ca^{2+} influx. (A–C) Time course of peak specific force recorded in EDL muscles from WT and CASQ1-null mice during 40 consecutive stimulus trains in the presence of either standard Ringer's solution containing 2.5 mM Ca^{2+} (A), nominally Ca^{2+} -free Ringer's solution (B), or standard Ringer's solution supplemented with 10 μM BTP-2 (C). **(D–F)** Quantitative analyses of the relative decay during the second stimulus train ($\text{ST}_{2\text{nd}}/\text{ST}_{1\text{st}}$) and the peak of the bump phase ($\text{ST}_{\text{peak}}/\text{ST}_{2\text{nd}}$) from the corresponding data shown in A–C. Data are shown as mean \pm SEM; *, $P < 0.05$. Numbers in parentheses (n) indicate the number of EDL muscles analyzed. Number of mice: $n = 8$ WT, $n = 7$ CASQ1-null, A and D; $n = 7$ WT, $n = 6$ CASQ1-null, B and E; $n = 7$ WT, $n = 6$ CASQ1-null, C and F.

muscle fibers from CASQ1-null mice are subjected to tetanic stimulation (Paolini et al., 2007; Canato et al., 2010). In the present work, we show that muscle fibers from sedentary CASQ1-null mice (e.g., not subjected to acute running on the treadmill) contain preassembled junctions between SR stacks and TT extensions within the I band of sarcomere (Fig. 1, Fig. 2, and Fig. S1) that resemble CEUs formed in WT mice after acute exercise (Boncompagni et al., 2017; Michelucci et al., 2019). Consistent with the TT extensions into stacks of SR membranes within the I band reflecting an increase in CEUs in muscle from CASQ1-null mice, the normal localization of Orail at the triad in WT muscle is shifted to a more I-band localization in muscle from CASQ1-null mice (Fig. S5). This relocalization of Orail within the I band in muscle from CASQ1-null mice resembles that reported previously for muscle of WT mice after acute exercise (Boncompagni et al., 2017).

The presence of preassembled SR-TT junctions in muscle of CASQ1-null mice coincides with enhanced constitutive and store-dependent Ca^{2+} influx (Fig. 3) and increased expression of STIM1S, STIM1L, Orail, and SERCA (Fig. 4). The increased ability to recover Ca^{2+} from the extracellular space via SOCE promotes SR Ca^{2+} store refilling (Fig. 6) needed for sustained Ca^{2+} release

(Fig. 5) and force generation (Fig. 7) during repetitive stimulation. These findings are consistent with the idea that the SR-TT junctions within the I band of CASQ1-null mice represent preassembled CEUs that provide a preferential pathway for constitutive and store-operated Ca^{2+} influx, which potentially serves as a surrogate Ca^{2+} pool to compensate for the marked reduction in total Ca^{2+} store capacity caused by the lack of CASQ1 (Fig. 6, A and B). While CEUs in WT mice dynamically assemble following acute exercise and disassemble during recovery (Michelucci et al., 2019), constitutively formed CEUs in muscle of CASQ1-null mice may reflect an adaptation to an insufficient SR Ca^{2+} pool needed to maintain proper muscle function during prolonged periods of activity. As a key protein for SR Ca^{2+} storage and release in fast-twitch skeletal muscle, CASQ1 could impact signaling between the intracellular and extracellular Ca^{2+} pools. Since STIM1 functions as a luminal SR Ca^{2+} sensor, the reduction in total releasable Ca^{2+} content in muscle fibers from CASQ1-null mice (Fig. 6, A and B) would be expected to enhance STIM1 oligomerization, Orail activation, and SOCE with the marked reduction in SR luminal free Ca^{2+} levels that occurs during repetitive stimulation (Fig. 6 F).

How does CASQ1 deficiency lead to increased constitutive and store-operated Ca^{2+} entry?

Similar to muscle fibers from WT mice after acute exercise (Michelucci et al., 2019), muscle fibers from CASQ1-null mice contain a noticeable amount of preassembled CEUs that correlated with enhanced constitutive and store-operated Ca^{2+} entry. Both Ca^{2+} entry pathways are likely mediated by Orail channels since they are blocked by BTP-2 (Fig. S2) and absent in muscle fibers from Orail KO mice (Michelucci et al., 2019). As muscle from both exercise WT and CASQ1-null mice are enriched in CEUs, we propose that constitutive SOCE arises from Orail channels in the elongated TT within the I-band region of the sarcomere that couples with stacks of SR membranes forming CEUs. This idea is supported by the immunofluorescence measurements showing that Orail redistributes from primarily triad localization in muscle fibers from sedentary WT mice to the I band under conditions that promote CEU formation (e.g., acute exercise, CASQ1 deficiency; Boncompagni et al., 2017; Fig. S5, B and D).

How do muscle fibers from CASQ1-null mice exhibit constitutive SOCE in the presence of full SR Ca^{2+} stores as reported by DIER measurements? As one possibility, our DIER measurements likely do not specifically reflect local Ca^{2+} levels within the SR lumen of the CEU. Indeed, as shown in Fig. 6 C, the majority of the DIER signal in the fibers used in our experiments is localized to the triad junction, though this most likely reflects the larger total amount of SR at triads compared with CEUs rather than a preferential targeting of the probe. Consistent with this, we previously reported that the ratio between the amount of SR in triads and CEUs is 37:1 in EDL muscle from WT mice under control conditions (Boncompagni et al., 2017). However, as DIER is a soluble protein and SR luminal Ca^{2+} gradients are thought to be minimal (Pape et al., 2007), local SR depletion within the CEU would require specific mechanisms (e.g., high localized SR Ca^{2+} leak coupled with limited SERCA Ca^{2+} uptake) to provide a localized depletion signal to activate constitutive Ca^{2+} entry. Future studies designed to monitor luminal Ca^{2+} levels specifically within the CEU will be needed to determine if CEUs exhibit reduced luminal SR Ca^{2+} store content. Alternatively, muscle from CASQ1-null mice (and WT mice after acute exercise) might produce an activator of Orail channels that does not require SR Ca^{2+} store depletion.

Therefore, the preassembly of CEUs in muscle of CASQ1-null mice may reflect a long-term post-natal adaptation that coincides with increased expression of STIM1S, STIM1L, Orail, and SERCA needed to enhance constitutive/store-operated Ca^{2+} influx and SR Ca^{2+} store refilling during repetitive stimulation. These results are in contrast with that reported previously, in which transient knockdown (2 wk) of CASQ1 resulted in a reduction in Orail and STIM1 expression (Zhao et al., 2010). This apparent discrepancy may be due to differential adaptations/compensations resulting from the constitutive absence of CASQ1 throughout development and maturation of muscle fibers into adulthood in our studies versus transient short hairpin RNA-mediated knockdown in young adult mice used by Zhao et al. (2010). The observed increase in STIM1, Orail, and SERCA expression and up-regulation of SOCE activity in CASQ1-null mice

could reflect a compensation for the loss of a protein critical in controlling releasable SR Ca^{2+} levels in muscle. On the other hand, a reduction in Orail expression following acute knockdown of CASQ1 in adult mice would be expected to limit SOCE activity, protecting muscle fibers from damage due to excessive Ca^{2+} influx (Zhao et al., 2010).

Ca^{2+} entry is essential for sustained contractile function in muscle of CASQ1-null mice

Despite a massive reduction of total releasable Ca^{2+} store content in muscle fibers from CASQ1-null mice, the peak amplitude of Ca^{2+} release and specific force production is normal during the first stimulus train. Thus, free SR Ca^{2+} concentration under resting conditions, which is increased in muscle fibers from CASQ1-null mice, is sufficient to support normal peak Ca^{2+} release and contractility during the first stimulus train (Canato et al., 2010; Sztrettye et al., 2011a). However, due to the combined effects of greater SR evacuability (Royer et al., 2010), marked reduction in total releasable Ca^{2+} store content, and decrease in luminal free Ca^{2+} concentration during electrical stimulation (Canato et al., 2010), peak Ca^{2+} transient amplitude is dramatically reduced during the second stimulus train. On the other hand, the drop in myoplasmic Ca^{2+} transient amplitude and specific force production in WT mice during the second transient is minimal, presumably due to normal SR evacuability, Ca^{2+} storage, and limited reduction in luminal free Ca^{2+} . Consistent with this, DIER measurements during repetitive 50-Hz stimulation revealed only a minimal effect on the SR Ca^{2+} levels in fibers from WT mice, but a large reduction in fibers from CASQ1-null mice. Our observations are in line with those published by Canato et al. (2010), although the changes in DIER ratio shown in Fig. 6 are somewhat smaller than those reported in that study. Two reasons may explain the lower change in DIER ratio in our experiments: (1) the different stimulation paradigms used (500 ms versus 2 s duration) and (2) the possible mislocalization of a fraction of the DIER probe in the myoplasm as previously demonstrated by Sztrettye et al. (2011a), which would reduce the relative magnitude of the change in signal within the SR lumen.

The deep reduction in luminal free Ca^{2+} during repetitive stimulation only in muscle fibers from CASQ1-null mice would be expected to activate SOCE. Indeed, the DIER signal remained constant in fibers from WT mice during repetitive stimulation but progressively increased in muscle fibers from CASQ1-null mice. This means that the activation of SOCE during repetitive contraction is significantly greater in muscle fibers from CASQ1-null mice than the WT. The critical role of SOCE in this progressive restoration of SR free Ca^{2+} is highlighted by the observation that BTP-2 treatment partially inhibited the progressive restoration of DIER signal. Specifically, while BTP-2 nearly abolished the bump phase of contraction during repetitive stimulation (Fig. 7 C), BTP-2 treatment did not completely eliminate SR Ca^{2+} refilling (Fig. 6 F). It is plausible that slower SR refilling observed in the presence of BTP-2 (and thus, absence of Orail-dependent Ca^{2+} entry) is not sufficient to support the rebound increase in specific force production. Moreover, the incomplete elimination of SR Ca^{2+} refilling

during repetitive stimulation by BTP-2 treatment indicates that BTP-2-insensitive Ca^{2+} influx pathways (e.g., CaV1.1) also contribute to SR Ca^{2+} refilling during repetitive stimulation in FDB fibers from CASQ1-null mice. Consistent with this idea, sustained Ca^{2+} transients and contractile function in muscle from JP45 and CASQ1 double KO mice depend on an enhancement of Ca^{2+} influx through skeletal muscle dihydropyridine receptor Ca^{2+} channels (CaV1.1 ; Mosca et al., 2013, 2016). These findings suggest that JP45 may be required for the enhancement of constitutive and store-operated Ca^{2+} entry observed in CASQ1-null mice and that Ca^{2+} entry through CaV1.1 is prioritized in the absence of JP45.

In our experiments, DIER-expressing fibers exhibited a clear striated triad fluorescence. Thus, we expect that the recorded signal was likely dominated by free Ca^{2+} levels within the terminal SR. However, dynamic changes in Ca^{2+} levels in different SR compartments (e.g., terminal SR, longitudinal SR, or CEUs) or, less likely, dynamic changes in DIER localization could impact the recorded signal and interpretation of results. For example, an increased DIER ratio could result from a transient increase in Ca^{2+} levels within SR stacks of the CEU. Nevertheless, consistent with a role for SOCE in store refilling in muscle from CASQ1-null mice during repetitive stimulation, BTP-2 abolished constitutive and store-operated Ca^{2+} entry and inhibited the bump phase of force production during repetitive stimulation. The difference in time course of SR store refilling (monotonic) and specific force production (biphasic) during repetitive stimulation most likely reflects the fact that store refilling represents only one of several factors that underlie the decline in muscle force production during repetitive stimulation (including metabolic changes, reactive oxygen species generation, Ca-PO_4 precipitation, and action potential failure; Allen et al., 2008a, 2008b).

The reduction of the bump phase of specific force in EDL muscles of WT mice and its absence in muscles from CASQ1-null mice when Ca^{2+} entry is reduced (e.g., 0 Ca^{2+} or BTP-2), suggests that SOCE promotes SR Ca^{2+} refilling during repetitive stimulation. This idea is supported by previous observations that the bump phase of force production during repetitive stimulation is abolished in muscles from muscle-specific, inducible Orail KO mice and muscle-specific, dominant-negative Orail transgenic mice (Michelucci et al., 2019). The larger effect of BTP-2 or 0 Ca^{2+} perfusion on the bump phase of EDL contraction during repetitive stimulation in CASQ1-null mice compared with that of WT mice (Fig. 7, B and C) is likely due to the larger SOCE activity and greater dependence on Ca^{2+} entry in CASQ1-deficient muscle. Thus, even a partial reduction in SOCE in intact muscles by these interventions would be expected to result in a stronger overall impact on EDL muscle contractility during repetitive stimulation in CASQ1-null mice compared with WT mice. Moreover, the bump phase of both Ca^{2+} release and specific force production during repetitive stimulation is augmented under conditions where CEU incidence/size and SOCE activity are increased (e.g., both WT mice after acute exercise and CASQ1-null mice; Boncompagni et al., 2017; Michelucci et al., 2019). Together, our findings suggest that CASQ1-null mice compensate for a marked reduction in total SR Ca^{2+} content by

using extracellular Ca^{2+} via SOCE as an alternative Ca^{2+} source to dynamically refill Ca^{2+} stores needed to sustain Ca^{2+} release and muscle contractility during repetitive stimulation.

Role of CASQ1 in SOCE regulation

Prior studies proposed a direct retrograde regulatory signal from CASQ1 to SOCE proteins in muscle (Shin et al., 2003; Zhao et al., 2010). Specifically, overexpression of CASQ1 in myotubes enhances RyR1-mediated Ca^{2+} release, while suppressing SOCE in a manner that depends on the aspartate-rich region of CASQ1 (Shin et al., 2003). Consistent with this, (1) transient knockdown of CASQ1 in adult muscle fibers increases SOCE activity (Zhao et al., 2010); and (2) the rate of SOCE current activation induced by passive SR Ca^{2+} depletion during whole-cell patch clamp experiments is accelerated in myotubes from CASQ1/2 double KO mice (Yarotskyy et al., 2013). As a potential mechanism, CASQ1 depolymerization during store depletion (Manno et al., 2013, 2017) was proposed to result in CASQ1 monomers that can interact with STIM1 in a manner that prevents STIM1 aggregation and subsequent Orail activation (Wang et al., 2015; Zhang et al., 2016). Such an inhibitory role of CASQ1 on SOCE activation could represent a protective mechanism designed to prevent exaggerated Ca^{2+} entry under physiological conditions. Thus, the enhanced constitutive and store-operated Ca^{2+} entry observed in fibers from CASQ1-null mice reported here could reflect the combined effects of preassembled CEUs, increased STIM1/Orail expression, enhanced susceptibility to activity-dependent store depletion, and reduced CASQ1-mediated inhibition of STIM1 aggregation and Orail activation.

Conclusions and implications

Results presented here support the idea that SR-TT junctions within the I-band region of the sarcomere function as CEUs that mediate STIM1/Orail-dependent constitutive and store-operated Ca^{2+} entry. An additional important finding of this study is that sustained Ca^{2+} transient amplitude and muscle force production during repetitive stimulation in muscle from CASQ1-null mice depend strongly on extracellular Ca^{2+} . This increased dependence on Ca^{2+} entry presumably reflects a long-term adaptation designed to compensate for a massive reduction of total store Ca^{2+} content and enhanced susceptibility of the SR to depletion during muscle activity. The presence of constitutively assembled CEUs in muscle of CASQ1-null mice could explain how these mice are able to survive despite the absence of a protein that was once presumed to be essential for skeletal muscle function.

Acknowledgments

Eduardo Ríos served as editor.

This work was supported by grants from the National Institutes of Health (AR059646 to R.T. Dirksen and subcontract to F. Protasi), the Italian Ministry of Education, University, and Research (Projects of National Interest [PRIN] no. 2015ZZR4W3 to F. Protasi), the Italian Telethon Non-Profit Organization Foundation (GGP13213 to F. Protasi), and the Alfred and Eleanor Wedd Fund (to A. Michelucci).

The authors declare no competing financial interests.

Author contributions: A. Michelucci designed and performed experiments, analyzed and interpreted data, and wrote and edited the manuscript. S. Boncompagni designed and performed experiments, analyzed and interpreted data, and wrote and edited the manuscript. L. Pietrangelo designed and performed experiments and analyzed data. T. Takano designed and performed experiments and analyzed data. F. Protasi designed experiments, interpreted data, and wrote and edited the manuscript. R.T. Dirksen designed experiments, interpreted data, and wrote and edited the manuscript.

Submitted: 26 March 2020

Accepted: 15 July 2020

References

- Allen, D.G., G.D. Lamb, and H. Westerblad. 2008b. Impaired calcium release during fatigue. *J. Appl. Physiol.* 104:296–305. <https://doi.org/10.1152/japplphysiol.00908.2007>
- Allen, D.G., G.D. Lamb, and H. Westerblad. 2008a. Skeletal muscle fatigue: cellular mechanisms. *Physiol. Rev.* 88:287–332. <https://doi.org/10.1152/physrev.00015.2007>
- Barone, V., V. Del Re, A. Gamberucci, V. Polverino, L. Galli, D. Rossi, E. Costanzi, L. Toniolo, G. Berti, A. Malandrini, et al. 2017. Identification and characterization of three novel mutations in the CASQ1 gene in four patients with tubular aggregate myopathy. *Hum. Mutat.* 38:1761–1773. <https://doi.org/10.1002/humu.23338>
- Beard, N.A., M.M. Sakowska, A.F. Dulhunty, and D.R. Laver. 2002. Calsequestrin is an inhibitor of skeletal muscle ryanodine receptor calcium release channels. *Biophys. J.* 82:310–320. [https://doi.org/10.1016/S0006-3495\(02\)75396-4](https://doi.org/10.1016/S0006-3495(02)75396-4)
- Boncompagni, S., F. Protasi, and C. Franzini-Armstrong. 2012. Sequential stages in the age-dependent gradual formation and accumulation of tubular aggregates in fast twitch muscle fibers: SERCA and calsequestrin involvement. *Age (Dordr.)* 34:27–41. <https://doi.org/10.1007/s11357-011-9211-y>
- Boncompagni, S., A. Michelucci, L. Pietrangelo, R.T. Dirksen, and F. Protasi. 2017. Exercise-dependent formation of new junctions that promote STIM1-Orail assembly in skeletal muscle. *Sci. Rep.* 7:14286. <https://doi.org/10.1038/s41598-017-14134-0>
- Boncompagni, S., A. Michelucci, L. Pietrangelo, R.T. Dirksen, and F. Protasi. 2018. Addendum: Exercise-dependent formation of new junctions that promote STIM1-Orail assembly in skeletal muscle. *Sci. Rep.* 8:17463. <https://doi.org/10.1038/s41598-018-33063-0>
- Campbell, K.P., D.H. MacLennan, A.O. Jorgensen, and M.C. Mintzer. 1983. Purification and characterization of calsequestrin from canine cardiac sarcoplasmic reticulum and identification of the 53,000 dalton glycoprotein. *J. Biol. Chem.* 258:1197–1204.
- Canato, M., M. Scorzeto, M. Giacomello, F. Protasi, C. Reggiani, and G.J. Stienen. 2010. Massive alterations of sarcoplasmic reticulum free calcium in skeletal muscle fibers lacking calsequestrin revealed by a genetically encoded probe. *Proc. Natl. Acad. Sci. USA.* 107:22326–22331. <https://doi.org/10.1073/pnas.1009168108>
- Capote, J., P. Bolaños, R.P. Schuhmeier, W. Melzer, and C. Caputo. 2005. Calcium transients in developing mouse skeletal muscle fibres. *J. Physiol.* 564:451–464. <https://doi.org/10.1113/jphysiol.2004.081034>
- Carrell, E.M., A.R. Coppola, H.J. McBride, and R.T. Dirksen. 2016. Orail enhances muscle endurance by promoting fatigue-resistant type I fiber content but not through acute store-operated Ca^{2+} entry. *FASEB J.* 30:4109–4119. <https://doi.org/10.1096/fj.201600621R>
- Cully, T.R., and B.S. Launikonis. 2013. Store-operated Ca^{2+} entry is not required for store refilling in skeletal muscle. *Clin. Exp. Pharmacol. Physiol.* 40:338–344. <https://doi.org/10.1111/1440-1681.12078>
- Dainese, M., M. Quarta, A.D. Lyfenko, C. Paolini, M. Canato, C. Reggiani, R.T. Dirksen, and F. Protasi. 2009. Anesthetic- and heat-induced sudden death in calsequestrin-1-knockout mice. *FASEB J.* 23:1710–1720. <https://doi.org/10.1096/fj.08-121335>
- Dirksen, R.T.. 2009. Checking your SOCCs and feet: the molecular mechanisms of Ca^{2+} entry in skeletal muscle. *J. Physiol.* 587:3139–3147. <https://doi.org/10.1113/jphysiol.2009.172148>
- Feske, S., Y. Gwack, M. Prakriya, S. Srikanth, S.H. Puppel, B. Tanasa, P.G. Hogan, R.S. Lewis, M. Daly, and A. Rao. 2006. A mutation in Orail causes immune deficiency by abrogating CRAC channel function. *Nature.* 441:179–185. <https://doi.org/10.1038/nature04702>
- Guarnier, F.A., A. Michelucci, M. Serano, L. Pietrangelo, C. Pecorai, S. Boncompagni, and F. Protasi. 2018. Aerobic Training Prevents Heatstrokes in Calsequestrin-1 Knockout Mice by Reducing Oxidative Stress. *Oxid. Med. Cell. Longev.* 2018:4652480. <https://doi.org/10.1155/2018/4652480>
- Hopf, F.W., P. Reddy, J. Hong, and R.A. Steinhardt. 1996. A capacitative calcium current in cultured skeletal muscle cells is mediated by the calcium-specific leak channel and inhibited by dihydropyridine compounds. *J. Biol. Chem.* 271:22358–22367. <https://doi.org/10.1074/jbc.271.37.22358>
- Kurebayashi, N., and Y. Ogawa. 2001. Depletion of Ca^{2+} in the sarcoplasmic reticulum stimulates Ca^{2+} entry into mouse skeletal muscle fibres. *J. Physiol.* 533:185–199. <https://doi.org/10.1111/j.1469-7793.2001.0185b.x>
- Li, T., E.A. Finch, V. Graham, Z.S. Zhang, J.D. Ding, J. Burch, M. Oh-hora, and P. Rosenberg. 2012. STIM1- Ca^{2+} signaling is required for the hypertrophic growth of skeletal muscle in mice. *Mol. Cell. Biol.* 32:3009–3017. <https://doi.org/10.1128/MCB.06599-11>
- Liou, J., M.L. Kim, W.D. Heo, J.T. Jones, J.W. Myers, J.E. Ferrell, Jr., and T. Meyer. 2005. STIM is a Ca^{2+} sensor essential for Ca^{2+} -store-depletion-triggered Ca^{2+} influx. *Curr. Biol.* 15:1235–1241. <https://doi.org/10.1016/j.cub.2005.05.055>
- Loy, R.E., M. Orynbayev, L. Xu, Z. Andronache, S. Apostol, E. Zvaritch, D.H. MacLennan, G. Meissner, W. Melzer, and R.T. Dirksen. 2011. Muscle weakness in $\text{Ryrl}^{14895T/WT}$ knock-in mice as a result of reduced ryanodine receptor Ca^{2+} ion permeation and release from the sarcoplasmic reticulum. *J. Gen. Physiol.* 137:43–57. <https://doi.org/10.1085/jgp.201010523>
- Lyfenko, A.D., and R.T. Dirksen. 2008. Differential dependence of store-operated and excitation-coupled Ca^{2+} entry in skeletal muscle on STIM1 and Orail. *J. Physiol.* 586:4815–4824. <https://doi.org/10.1113/jphysiol.2008.160481>
- Manno, C., L. Figueroa, L. Royer, S. Pouvreau, C.S. Lee, P. Volpe, A. Nori, J. Zhou, G. Meissner, S.L. Hamilton, et al. 2013. Altered Ca^{2+} concentration, permeability and buffering in the myofibre Ca^{2+} store of a mouse model of malignant hyperthermia. *J. Physiol.* 591:4439–4457. <https://doi.org/10.1113/jphysiol.2013.259572>
- Manno, C., L.C. Figueroa, D. Gillespie, R. Fitts, C. Kang, C. Franzini-Armstrong, and E. Rios. 2017. Calsequestrin depolymerizes when calcium is depleted in the sarcoplasmic reticulum of working muscle. *Proc. Natl. Acad. Sci. USA.* 114:E638–E647. <https://doi.org/10.1073/pnas.1620265114>
- Michelucci, A., C. Paolini, M. Canato, L. Wei-Lapierre, L. Pietrangelo, A. De Marco, C. Reggiani, R.T. Dirksen, and F. Protasi. 2015. Antioxidants protect calsequestrin-1 knockout mice from halothane- and heat-induced sudden death. *Anesthesiology.* 123:603–617. <https://doi.org/10.1097/ALN.0000000000000748>
- Michelucci, A., C. Paolini, S. Boncompagni, M. Canato, C. Reggiani, and F. Protasi. 2017. Strenuous exercise triggers a life-threatening response in mice susceptible to malignant hyperthermia. *FASEB J.* 31:3649–3662. <https://doi.org/10.1096/fj.201601292R>
- Michelucci, A., M. García-Castañeda, S. Boncompagni, and R.T. Dirksen. 2018. Role of STIM1/ORAI1-mediated store-operated Ca^{2+} entry in skeletal muscle physiology and disease. *Cell Calcium.* 76:101–115. <https://doi.org/10.1016/j.ceca.2018.10.004>
- Michelucci, A., S. Boncompagni, L. Pietrangelo, M. García-Castañeda, T. Takano, S. Malik, R.T. Dirksen, and F. Protasi. 2019. Transverse tubule remodeling enhances Orail-dependent Ca^{2+} entry in skeletal muscle. *eLife.* 8:e47576. <https://doi.org/10.7554/eLife.47576>
- Mosca, B., O. Delbono, M. Laura Messi, L. Bergamelli, Z.M. Wang, M. Vukcevic, R. Lopez, S. Treves, M. Nishi, H. Takeshima, et al. 2013. Enhanced dihydropyridine receptor channel activity restores muscle strength in JP45/CASQ1 double knockout mice. *Nat. Commun.* 4:1541. <https://doi.org/10.1038/ncomms2496>
- Mosca, B., J. Eckhardt, L. Bergamelli, S. Treves, R. Bongianino, M. De Negri, S.G. Priori, F. Protasi, and F. Zorzato. 2016. Role of the JP45-calsequestrin complex on calcium entry in slow twitch skeletal muscles. *J. Biol. Chem.* 291:20824. <https://doi.org/10.1074/jbc.A115.709071>
- Paolini, C., M. Quarta, A. Nori, S. Boncompagni, M. Canato, P. Volpe, P.D. Allen, C. Reggiani, and F. Protasi. 2007. Reorganized stores and impaired calcium handling in skeletal muscle of mice lacking calsequestrin-1. *J. Physiol.* 583:767–784. <https://doi.org/10.1113/jphysiol.2007.138024>
- Paolini, C., M. Quarta, L. Wei-LaPierre, A. Michelucci, A. Nori, C. Reggiani, R.T. Dirksen, and F. Protasi. 2015. Oxidative stress, mitochondrial

- damage, and cores in muscle from calsequestrin-1 knockout mice. *Skelet. Muscle*. 5:10. <https://doi.org/10.1186/s13395-015-0035-9>
- Pape, P.C., K. Fénelon, C.R. Lamboley, and D. Stachura. 2007. Role of calsequestrin evaluated from changes in free and total calcium concentrations in the sarcoplasmic reticulum of frog cut skeletal muscle fibres. *J. Physiol.* 581:319–367. <https://doi.org/10.1113/jphysiol.2006.126474>
- Prakriya, M., S. Peske, Y. Gwack, S. Srikanth, A. Rao, and P.G. Hogan. 2006. Orail is an essential pore subunit of the CRAC channel. *Nature*. 443: 230–233. <https://doi.org/10.1038/nature05122>
- Protasi, F., C. Paolini, and M. Dainese. 2009. Calsequestrin-1: a new candidate gene for malignant hyperthermia and exertional/environmental heat stroke. *J. Physiol.* 587:3095–3100. <https://doi.org/10.1113/jphysiol.2009.171967>
- Roos, J., P.J. DiGregorio, A.V. Yeromin, K. Ohlsen, M. Lioudyno, S. Zhang, O. Safrina, J.A. Kozak, S.L. Wagner, M.D. Cahalan, et al. 2005. STIM1, an essential and conserved component of store-operated Ca^{2+} channel function. *J. Cell Biol.* 169:435–445. <https://doi.org/10.1083/jcb.200502019>
- Royer, L., M. Sztryte, C. Manno, S. Pouvreau, J. Zhou, B.C. Knollmann, F. Protasi, P.D. Allen, and E. Ríos. 2010. Paradoxical buffering of calcium by calsequestrin demonstrated for the calcium store of skeletal muscle. *J. Gen. Physiol.* 136:325–338. <https://doi.org/10.1085/jgp.201010454>
- Shin, D.W., Z. Pan, E.K. Kim, J.M. Lee, M.B. Bhat, J. Parness, D.H. Kim, and J. Ma. 2003. A retrograde signal from calsequestrin for the regulation of store-operated Ca^{2+} entry in skeletal muscle. *J. Biol. Chem.* 278: 3286–3292. <https://doi.org/10.1074/jbc.M209045200>
- Stiber, J., A. Hawkins, Z.S. Zhang, S. Wang, J. Burch, V. Graham, C.C. Ward, M. Seth, E. Finch, N. Malouf, et al. 2008. STIM1 signalling controls store-operated calcium entry required for development and contractile function in skeletal muscle. *Nat. Cell Biol.* 10:688–697. <https://doi.org/10.1038/ncb1731>
- Sztryte, M., J. Yi, L. Figueroa, J. Zhou, L. Royer, and E. Ríos. 2011a. D4cpv-calsequestrin: a sensitive ratiometric biosensor accurately targeted to the calcium store of skeletal muscle. *J. Gen. Physiol.* 138:211–229. <https://doi.org/10.1085/jgp.201010591>
- Sztryte, M., J. Yi, L. Figueroa, J. Zhou, L. Royer, P. Allen, G. Brum, and E. Ríos. 2011b. Measurement of RyR permeability reveals a role of calsequestrin in termination of SR Ca^{2+} release in skeletal muscle. *J. Gen. Physiol.* 138:231–247. <https://doi.org/10.1085/jgp.201010592>
- Sztryte, M., N. Geyer, J. Vincze, D. Al-Gaadi, T. Oláh, P. Szentesi, G. Kis, M. Antal, I. Balatoni, L. Csernoch, et al. 2017. SOCE is important for maintaining sarcoplasmic calcium content and release in skeletal muscle fibers. *Biophys. J.* 113:2496–2507. <https://doi.org/10.1016/j.bpj.2017.09.023>
- Vig, M., C. Peinelt, A. Beck, D.L. Koomoa, D. Rabah, M. Koblan-Huberson, S. Kraft, H. Turner, A. Fleig, R. Penner, et al. 2006. CRACM1 is a plasma membrane protein essential for store-operated Ca^{2+} entry. *Science*. 312: 1220–1223. <https://doi.org/10.1126/science.1127883>
- Wang, L., L. Zhang, S. Li, Y. Zheng, X. Yan, M. Chen, H. Wang, J.W. Putney, and D. Luo. 2015. Retrograde regulation of STIM1-Orail interaction and store-operated Ca^{2+} entry by calsequestrin. *Sci. Rep.* 5:11349. <https://doi.org/10.1038/srep11349>
- Wei-Lapierre, L., E.M. Carrell, S. Boncompagni, F. Protasi, and R.T. Dirksen. 2013. Orail-dependent calcium entry promotes skeletal muscle growth and limits fatigue. *Nat. Commun.* 4:2805. <https://doi.org/10.1038/ncomms3805>
- Yano, K., and A. Zarain-Herzberg. 1994. Sarcoplasmic reticulum calsequestrins: structural and functional properties. *Mol. Cell. Biochem.* 135:61–70. <https://doi.org/10.1007/BF00925961>
- Yarotsky, V., F. Protasi, and R.T. Dirksen. 2013. Accelerated activation of SOCE current in myotubes from two mouse models of anesthetic- and heat-induced sudden death. *PLoS One*. 8. e77633. <https://doi.org/10.1371/journal.pone.0077633>
- Yeromin, A.V., S.L. Zhang, W. Jiang, Y. Yu, O. Safrina, and M.D. Cahalan. 2006. Molecular identification of the CRAC channel by altered ion selectivity in a mutant of Orail. *Nature*. 443:226–229. <https://doi.org/10.1038/nature05108>
- Zhang, S.L., Y. Yu, J. Roos, J.A. Kozak, T.J. Deerinck, M.H. Ellisman, K.A. Stauderman, and M.D. Cahalan. 2005. STIM1 is a Ca^{2+} sensor that activates CRAC channels and migrates from the Ca^{2+} store to the plasma membrane. *Nature*. 437:902–905. <https://doi.org/10.1038/nature04147>
- Zhang, L., L. Wang, S. Li, J. Xue, and D. Luo. 2016. Calsequestrin-1 regulates store-operated Ca^{2+} entry by inhibiting STIM1 aggregation. *Cell. Physiol. Biochem.* 38:2183–2193. <https://doi.org/10.1159/000445574>
- Zhao, X., C.K. Min, J.K. Ko, J. Parness, D.H. Kim, N. Weisleder, and J. Ma. 2010. Increased store-operated Ca^{2+} entry in skeletal muscle with reduced calsequestrin-1 expression. *Biophys. J.* 99:1556–1564. <https://doi.org/10.1016/j.bpj.2010.06.050>
- Ziman, A.P., C.W. Ward, G.G. Rodney, W.J. Lederer, and R.J. Bloch. 2010. Quantitative measurement of Ca^{2+} in the sarcoplasmic reticulum lumen of mammalian skeletal muscle. *Biophys. J.* 99:2705–2714. <https://doi.org/10.1016/j.bpj.2010.08.032>
- Zitt, C., B. Strauss, E.C. Schwarz, N. Spaeth, G. Rast, A. Hatzelmann, and M. Hoth. 2004. Potent inhibition of Ca^{2+} release-activated Ca^{2+} channels and T-lymphocyte activation by the pyrazole derivative BTP2. *J. Biol. Chem.* 279:12427–12437. <https://doi.org/10.1074/jbc.M309297200>

Supplemental material

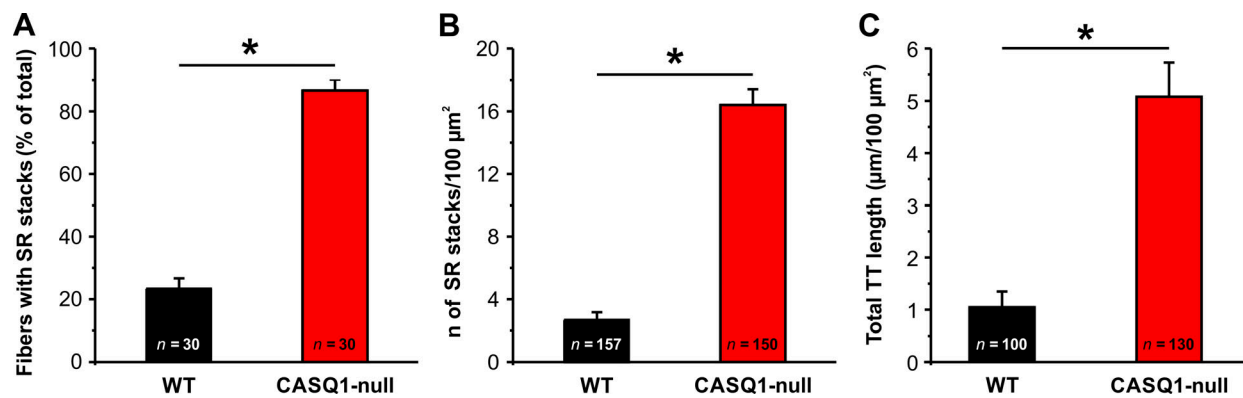


Figure S1. **SR stack incidence, number/area, and TT extension in FDB muscle fibers.** (A–C) Quantitative analyses of the percentage of muscle fibers exhibiting SR stacks (A), number of SR stacks per 100 μm^2 of cross-sectional area (B), and TT length in the I band ($\mu\text{m}/100 \mu\text{m}^2$ of cross-sectional area; C) determined from longitudinal sections of FDB muscle fibers from WT and CASQ1-null mice. Data are shown as mean \pm SEM; *, $P < 0.05$. Numbers in bars (n) indicate the number of FDB fibers analyzed. Number of mice: $n = 3$ WT; $n = 3$ CASQ1-null.

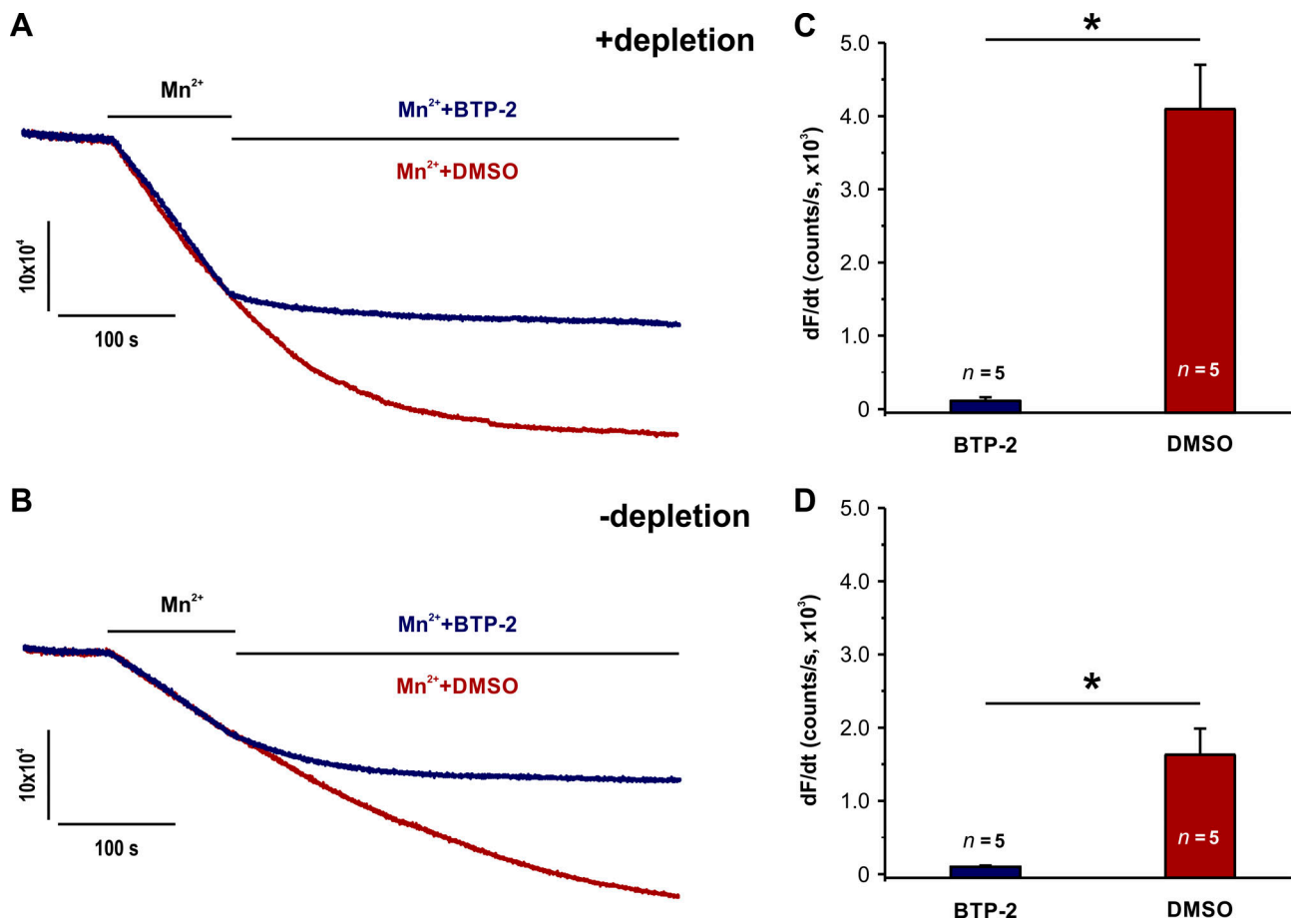


Figure S2. **BTP-2 sensitivity of store-operated and constitutive Mn^{2+} quench in FDB fibers.** (A–D) Representative superimposed traces of fura-2 fluorescence (A and B) and quantitative analyses of the maximum rate of Mn^{2+} quench (C and D) during application of 0.5 mM Mn^{2+} followed by 0.5 mM Mn^{2+} supplemented with either 10 μ M BTP-2 (blue) or DMSO (red) vehicle in FDB fibers from CASQ1-null mice in the presence (+depletion; A and C) or absence (–depletion; B and D) of prior store depletion. Data are shown as mean \pm SEM; *, $P < 0.05$. Numbers in bars (n) indicate the number of FDB fibers analyzed. Number of mice: n = 2 CASQ1-null.

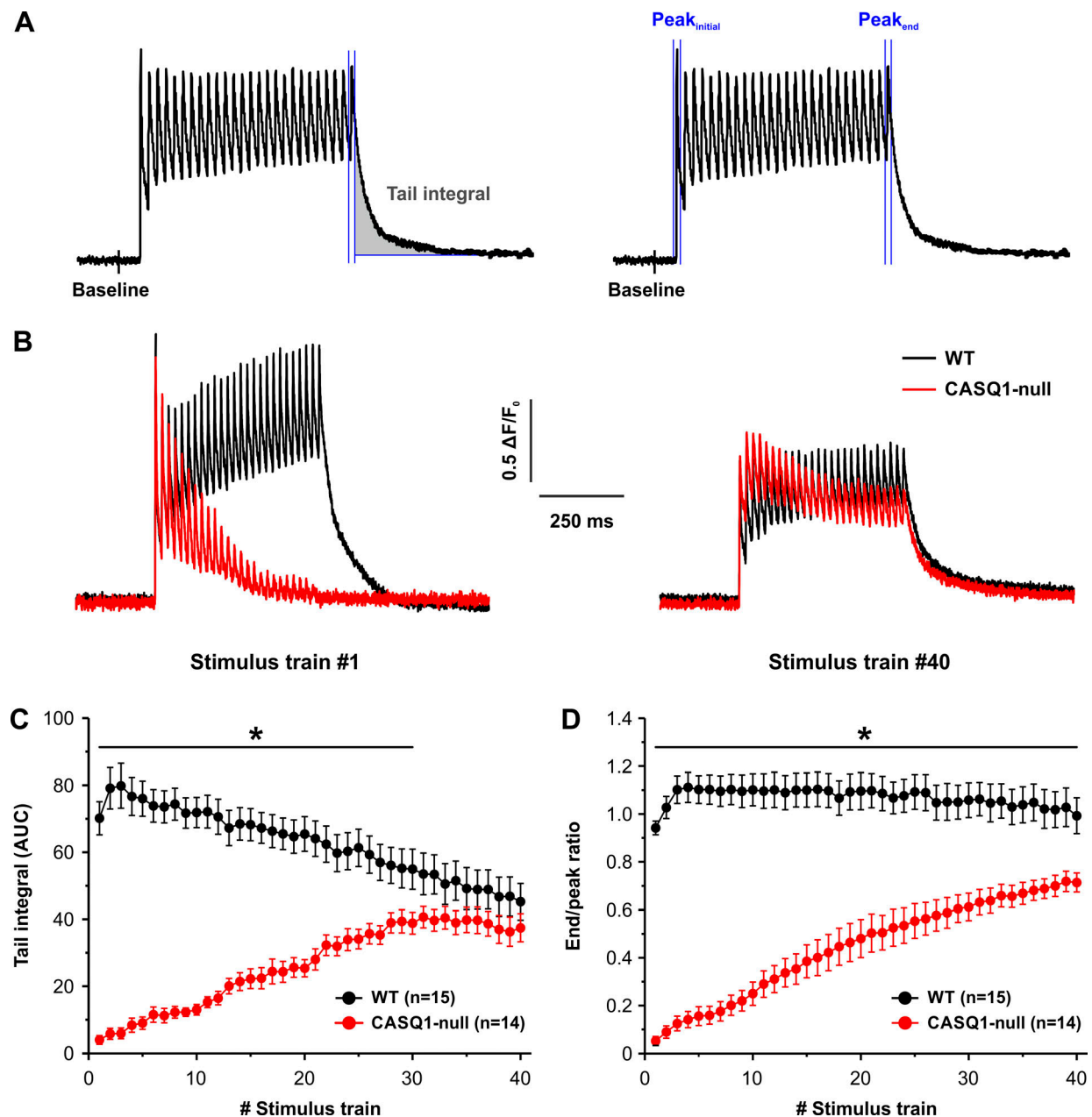


Figure S3. **Tail integral and end/peak ratio during repetitive stimulation.** (A) Representative mag-fluo-4 fluorescence trace elicited during a single stimulus train (500 ms at 50 Hz) highlighting analysis of tail integral (left, gray shaded area) and end/peak ratio (right). (B) Representative superimposed mag-fluo-4 ($\Delta F/F_0$) traces during the 1st (left) and 40th (right) stimulus train in FDB fibers isolated from WT and CASQ1-null mice. (C and D) Ca^{2+} transient tail integral (C) and end/peak ratio (D) analyses in FDB fibers from WT and CASQ1-null mice. Data are shown as mean \pm SEM; *, $P < 0.05$. Numbers in parentheses (n) indicate the number of FDB fibers analyzed. Number of mice: $n = 4$ WT; $n = 5$ CASQ1-null. AUC, area under the curve.

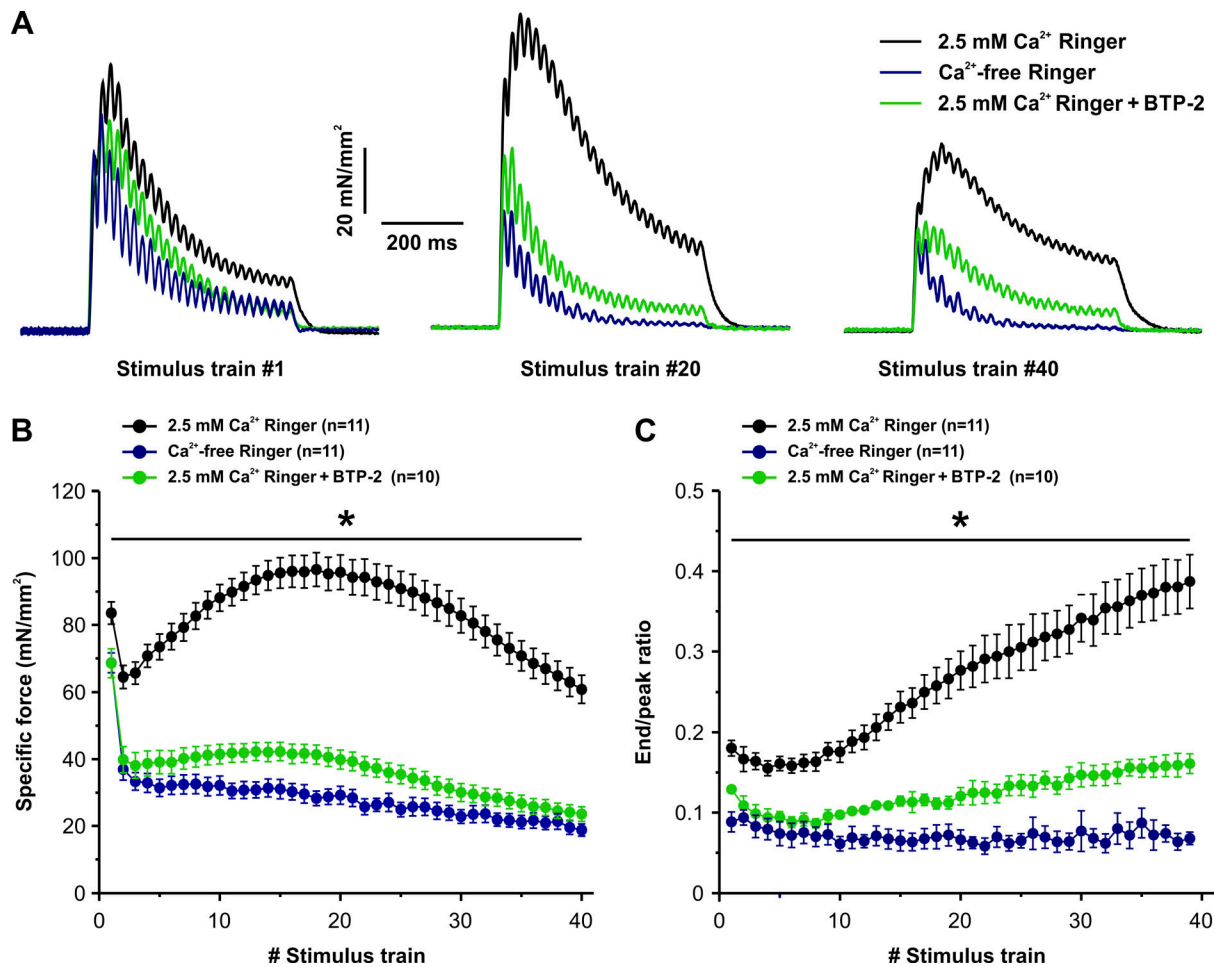


Figure S4. **Contractile force and decay during repetitive stimulation in the presence or absence of Ca^{2+} influx.** (A) Representative superimposed specific force traces elicited during the 1st (left), 20th (middle), and 40th (right) stimulus train in EDL muscles from CASQ1-null mice conducted in either standard Ringer's solution containing 2.5 mM Ca^{2+} (black), nominally Ca^{2+} -free Ringer's (blue), or standard Ringer's solution supplemented with 10 μM BTP-2 (green). (B and C) Time course analyses of specific force (B) and end/peak ratio (C) under the three different experimental conditions. Data are shown as mean \pm SEM; *, $P < 0.05$. Numbers in parentheses (n) indicate the number of EDL muscles analyzed. Number of mice: $n = 6$ CASQ1-null (2.5 mM Ca^{2+}); $n = 6$ CASQ1-null (Ca^{2+} -free); $n = 7$ CASQ1-null (2.5 mM Ca^{2+} + BTP-2).

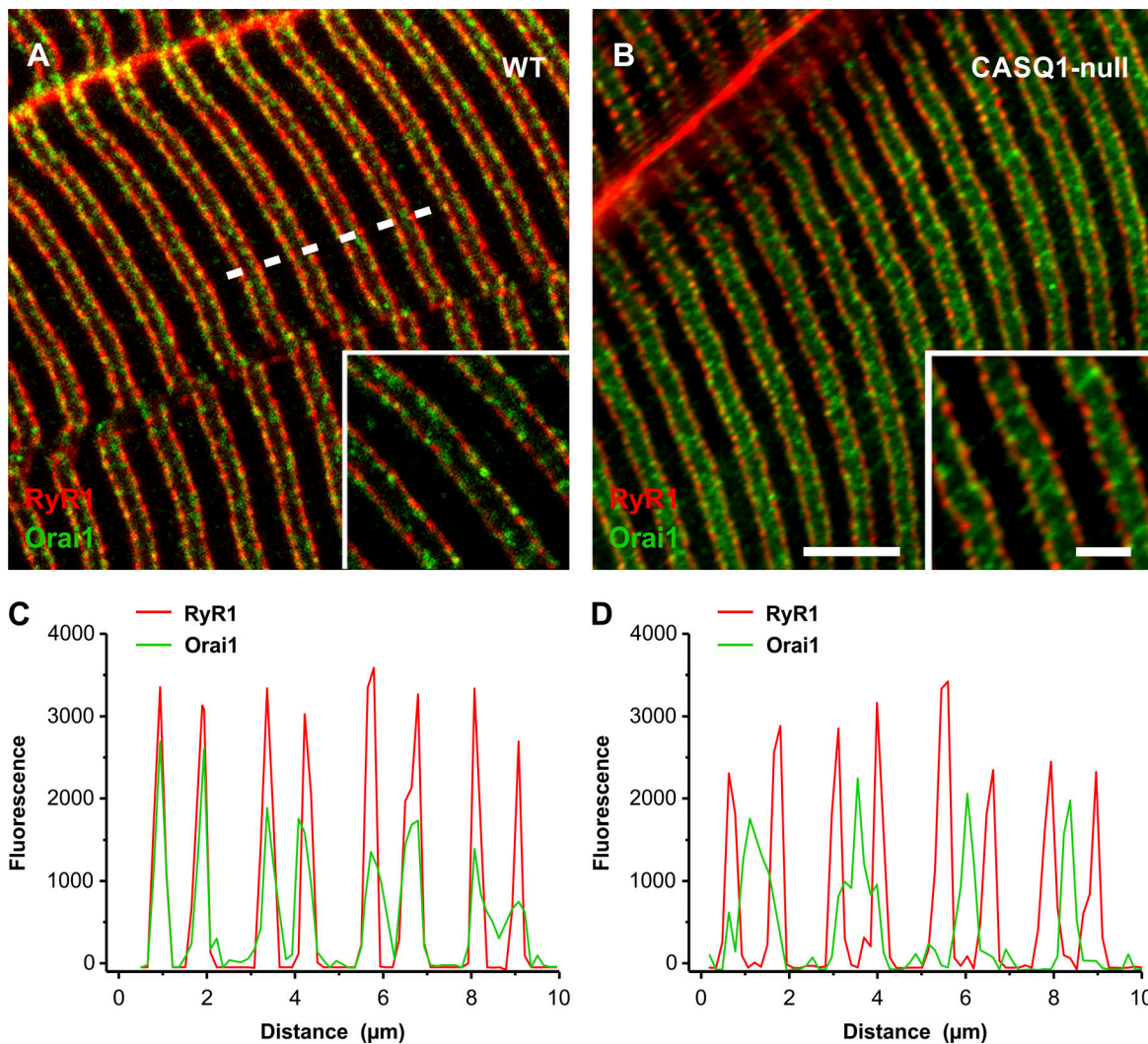


Figure S5. **Immunostaining for RyR1 and Orai1 in EDL fibers.** (A and B) Representative immunofluorescence images obtained in EDL fibers from WT (A) and CASQ1-null (B) mice that were double-labeled for RyR1 (red) and Orai1 (green). (C and D) Fluorescence intensity profiles along four sarcomeres for the EDL fibers from WT (C) and CASQ1-null (D) mice shown by the dashed line in A. Scale bar, 5 μm (inset, 1 μm).